JGR Oceans

RESEARCH ARTICLE
10.1029/2021JC018110

Key Points:

- Secular increases in particulate export and sedimentary denitrification (1988–2018) are correlated with increases in total annual NPP
- Export and denitrification are highest in years with dominant under-ice NPP; increases from January-June drive the increasing secular trends
- Increases in winter N concentrations contribute to further increases in denitrification, possibly affecting downstream NPP

Supporting Information:

Supporting Information may be found in the online version of this article.

Correspondence to:

C. M. Payne,
cmpayne@stanford.edu

Citation:

Payne, C. M., & Arrigo, K. R. (2022). Increases in benthic particulate export and sedimentary denitrification in the northern Chukchi Sea tied to under-ice primary production. *Journal of Geophysical Research: Oceans*, *127*, e2021JC018110. https://doi.org/10.1029/2021JC018110

Received 6 OCT 2021
Accepted 11 JAN 2022

Author Contributions:

Conceptualization: C. M. Payne, K. R. Arrigo
Formal analysis: C. M. Payne, K. R. Arrigo
Investigation: C. M. Payne, K. R. Arrigo
Methodology: C. M. Payne
Supervision: K. R. Arrigo
Validation: C. M. Payne
Visualization: C. M. Payne
Writing – original draft: C. M. Payne
Writing – review & editing: C. M. Payne, K. R. Arrigo

Increases in Benthic Particulate Export and Sedimentary Denitrification in the Northern Chukchi Sea Tied to Under-Ice Primary Production

C. M. Payne[1] and K. R. Arrigo[1]

[1]Department of Earth System Science, Stanford University, Stanford, CA, USA

Abstract Changing sea ice conditions have led to increases in net primary production (NPP) in the northern Chukchi Sea, driven in part by massive under-ice phytoplankton blooms. These blooms increase particle export to the sediments and could affect the rate of sedimentary denitrification. We use a 1-D coupled ecosystem model forced with satellite-derived sea ice conditions to quantify changes in particle export, nitrification, and denitrification on the northern Chukchi shelf. Between 1988 and 2018, increases in annual NPP drove secular increases in particle export to the benthos (1.8 ± 0.8 mmol m^{-2} yr^{-1}), water-column and sedimentary nitrification (1.2 ± 0.4 and 1.1 ± 0.4 mmol m^{-2} yr^{-1}, respectively), and sedimentary denitrification rates (1.3 ± 0.5 mmol m^{-2} yr^{-1}). Increased annual export to the benthos and denitrification were driven by higher rates early in the year (from January to June) and are highest in years where under-ice blooms (UIBs) dominate. Greater denitrification rates in the northern Chukchi Sea would likely reduce NPP in downstream regions such as the Greenland Sea and promote greater N_2 fixation in the North Atlantic. Furthermore, sea ice loss and a change in advection of nitrogen (N)-replete waters through the Bering Strait will likely increase winter N concentrations in the northern Chukchi Sea. Through N sensitivity experiments, we found that 30% of all added N was lost through denitrification, diminishing the N supply available downstream of the Chukchi Sea. Thus, increased particle export associated with UIBs has the potential to markedly alter the N cycle both in the northern Chukchi Sea and in adjacent waters.

Plain Language Summary As sea ice has thinned and retreated, phytoplankton blooms have changed in the Arctic Ocean. In the Chukchi Sea, large phytoplankton blooms have shifted earlier in the year and are even generated when the ocean is covered in sea ice, a period previously assumed to be too light-limited to allow for blooms. We use a 1-D model to understand how changes in phytoplankton productivity could influence the nitrogen (N) cycle in the northern Chukchi Sea. We found that increasing under-ice blooms (UIB) have led to increases in the export of particles to the sediments, which has subsequently led to an increase in both N recycling (nitrification) and N loss (denitrification) in the sediments. The increases in N loss in the region would likely negatively affect downstream ecosystems, where there could be less N available. We also investigated how a change in N supply to the region might affect phytoplankton blooms and the N cycle. We found that 30% of all added N was lost through denitrification, which would also diminish the N available downstream of the Chukchi Sea. By increasing the export of particles to the seafloor, UIBs can markedly alter the N cycle both in the Chukchi Sea and in downstream waters.

1. Introduction

The Chukchi Sea, located north of the Bering Strait, is one of the most productive regions in the Arctic Ocean. Mean estimates of annual net primary production (NPP) for the region typically range between 55 and 105 g C m^{-2} yr^{-1} (Arrigo et al., 2014; Hill & Cota, 2005; Lee et al., 2007). Along major advective pathways, however, particularly high nutrient concentrations can spur rates of NPP that surpass 170 g C m^{-2} yr^{-1} (Hansell et al., 1993; Hill, Light, et al., 2018). This high NPP supports substantial zooplankton, fish, seabird, and marine mammal populations (De Robertis et al., 2017; Ershova et al., 2015; Kuletz et al., 2015; Logerwell et al., 2015; Moore & Kuletz, 2019) as well as rich benthic communities (Grebmeier, 2006; Grebmeier et al., 1988, 2015; Lalande et al., 2007).

In recent decades, earlier onset of sea ice melt and retreat as well as later sea ice advance in the Chukchi Sea (Stroeve et al., 2014) have contributed to a 34% increase in the length of the ice-free period between 1998 and 2018 (Lewis et al., 2020). The sea ice in the region has also thinned substantially in recent decades; Kwok (2018)

found a nearly 50% decline in ice thickness in the northern Chukchi Sea between 1958 and 1997 (from 2 to 1 m), and a further 40% decline in ice thickness between 1997 and 2017 (from 1 to 0.6 m). Serreze and Stroeve (2015) use ice age as a proxy for thickness but come to a similar conclusion, finding that only 5% of the Arctic was covered in ice more than 5 years old in 2014, as compared to nearly 30% in 1988.

Changes in sea ice coverage have affected Chukchi Sea ecosystems. As sea ice extent diminished between 1998 and 2018, satellite-derived observations indicate that the Chukchi Sea has experienced a 30% increase in open water area and a 97% increase in annual NPP (Lewis et al., 2020). The delay in ice advance in autumn led to a 35% increase in the incidence of remotely sensed autumn blooms in the Chukchi Sea between 1998 and 2012 (Ardyna et al., 2014). Further, substantial phytoplankton blooms have been observed under fully consolidated ice cover in the Chukchi Sea (Arrigo et al., 2012, 2014; Hill, Light, et al., 2018). Model results by Horvat et al. (2017) found that these under-ice blooms (UIBs), likely a rare feature in the Arctic Ocean prior to 1990 (Ardyna et al., 2020), could have formed over as much as 30% of the Arctic Ocean between 2006 and 2015 as younger, thinner sea ice dominated the region. More frequent observations of UIBs throughout the Arctic Ocean in recent years (Arrigo et al., 2012, 2014; Assmy et al., 2017; Boles et al., 2020; Hill, Ardyna, et al., 2018; Leu et al., 2011; Mundy et al., 2009, 2014; Oziel et al., 2019; Randelhoff et al., 2020) indicate that these blooms may be becoming more frequent as sea ice conditions change.

Furthermore, climate change is likely to either diminish or enhance nutrient supply to the surface of the Arctic Ocean, thus changing annual NPP (Lewis et al., 2020; Li et al., 2009). Observations in the early 2010s indicated that nutrient entrainment in the surface ocean decreased due to an increase in precipitation, ice melt, and river outflow (McLaughlin & Carmack, 2010; Nummelin et al., 2016), causing smaller phytoplankton species to proliferate (Li et al., 2009). However, recent evidence indicates that substantial increases in NPP since 2012 (Henley et al., 2020; Lewis et al., 2020) have largely been promoted by an increase in nutrient supply (Lewis et al., 2020; Mordy et al., 2020; Randelhoff et al., 2019, 2020). These increases are likely a result of sea ice loss, as the greater open water area leads to more mixing events (Zhang et al., 2010), more storms (Yang, 2004), enhanced upwelling near shelf breaks (Carmack & Chapman, 2003; Tremblay et al., 2011; Tremblay & Gagnon, 2009), and the generation of internal waves (Rainville & Woodgate, 2009). In the Chukchi Sea, where the northward advection of NO_3^--replete waters through the Bering Strait predominates (Woodgate et al., 2005), changes in transport may also lead to changes in nutrient concentrations. Between 1990 and 2015, a strengthening of the Pacific-Arctic pressure head (Peralta-Ferriz & Woodgate, 2017) led to an increase in transport through the Bering Strait of 0.01 Sv yr^{-1} (Woodgate, 2018), corresponding to a 30% increase in transport over the climatology. High transport of Pacific waters into the Arctic Ocean has been associated with ship-based and mooring observations of higher nutrient concentrations in the Chukchi Sea (Mordy et al., 2020), indicating that nutrient concentrations may increase in the Chukchi Sea if this increase in transport continues.

Altered sea ice conditions and NPP could have substantial impacts on the marine nitrogen (N) cycle in the Chukchi Sea and further downstream (Arrigo et al., 2014; Arrigo & Van Dijken, 2015). Phytoplankton blooms in the under-ice (UI) period are dominated by diatoms (Laney & Sosik, 2014) which sink rapidly and contribute disproportionately to global particulate organic carbon (POC) export due to their highly silicified cell walls and large cell size (Smetacek, 1999). If NPP during the UI period is substantial, reduced grazing pressure due to cold water temperatures (Campbell et al., 2001; Coyle et al., 2007; Huntley & Lopez, 1992) is likely to increase POC and particulate organic N (PON) export to the sediments (Payne et al., 2021). Observations in the northern Chukchi Sea indicate that algal export during the UI period can be high (with daily chlorophyll (Chl) *a* export to the benthos of up to 5 mg m^{-3} d^{-1}), is almost entirely diatom-dominated (93%–100%), and has increased over time (Lalande et al., 2007, 2020; Szymanski & Gradinger, 2016). This observed increase in organic matter export to the sediments should substantially increase benthic-pelagic coupling (Honjo et al., 2010; Lalande et al., 2020) and could have implications for regional N loss. Coupled partial nitrification-denitrification in the sediments of the shallow Chukchi shelf (Brown et al., 2015) drives both high N recycling and high rates of fixed N loss in the sediments. As a result, the Chukchi Sea accounts for 1%–3% of the global sink of fixed N in the oceans (Chang & Devol, 2009). Both observational studies (Baumann et al., 2013; Granger et al., 2011; Horak et al., 2013; Townsend & Cammen, 1988) and models (Chang & Devol, 2009; Fennel, 2010; Fennel et al., 2009; Laurent et al., 2016; Soetaert et al., 1996a, 1996b) indicate that increases in particle export can lead to increases in sedimentary denitrification when other controls on denitrification (namely, bottom-water oxygen and N concentrations and water column depth; Soetaert et al., 1996a, 1996b) are constant. A further increase in sedimentary denitrification could

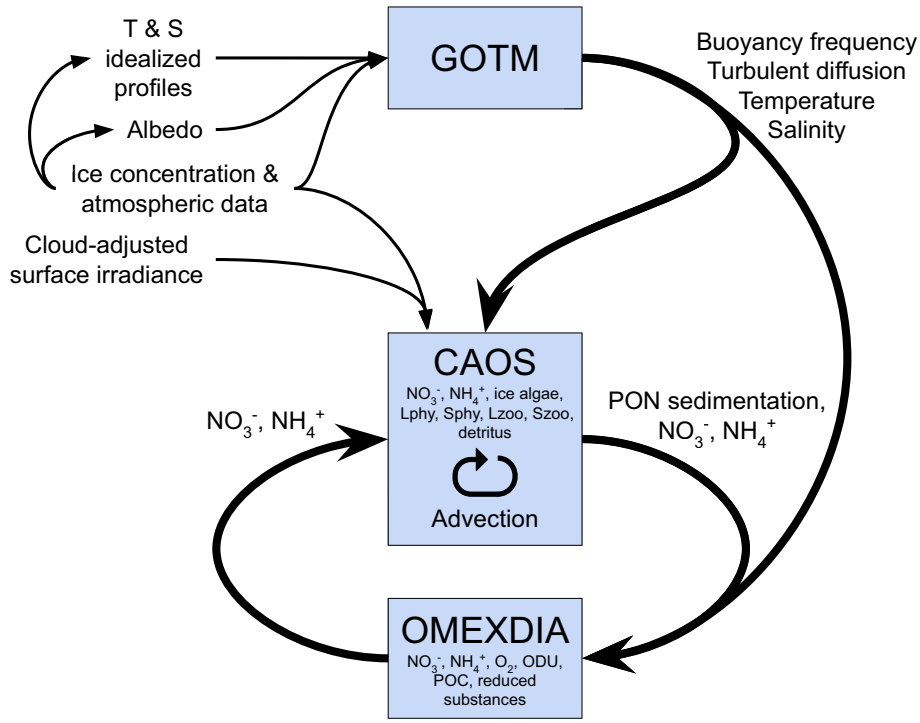

Figure 1. An overview of the inputs and outputs shared between the three coupled models (the General Ocean Turbulence Model, or GOTM; the Coupled Arctic Ocean System Model, or CAOS; and OMEXDIA) that form CAOS-GO. Thick lines represent flows between models, while thin lines represent external inputs to the models. State variables are listed in small text for the CAOS and OMEXDIA models. Lphy, Sphy, Lzoo, and Szoo are abbreviations for the CAOS model state variables of large phytoplankton, small phytoplankton, large zooplankton, and small zooplankton, respectively. ODU is an abbreviation for the OMEXDIA model state variable of oxygen demand units. From Payne et al. (2021).

also have some downstream impacts, potentially limiting NPP downstream of the Chukchi Sea (Arrigo & Van Dijken, 2015) but increasing rates of N_2 fixation in the North Atlantic (Yamamoto-Kawai et al., 2006).

To investigate the impacts of changing patterns of NPP in the Chukchi Sea between 1988 and 2018 on the regional N cycle, we use a coupled ecosystem model, CAOS-GO (the Coupled Arctic Ocean System model with GOTM and OMEXDIA; Payne et al., 2021), composed of interconnected biogeochemical (the Coupled Arctic Ocean System model, or CAOS; Payne et al., 2021), physical (the General Ocean Turbulence Model, or GOTM, version 5.4; Burchard et al., 1999), and sedimentary chemistry (OMEXDIA; Soetaert et al., 1996a, 1996b) models. We evaluate the impact of interannual changes in sea ice conditions and increasing annual NPP (Payne et al., 2021) on the export rate of PON from surface waters to the benthos and whether this export has stimulated or inhibited water column and sedimentary nitrification and denitrification. Further, we quantify the sensitivity of annual NPP, PON export, nitrification, and denitrification to changes in the N inventory of the Chukchi Sea.

2. Methods

2.1. Modeling Configuration

The coupled CAOS-GO model (Figure 1) was implemented at 72.16°N and 166.60°W (Figure 2) in the northern Chukchi Sea for the period 1988–2018, as in Payne et al. (2021). GOTM (Burchard et al., 1999) and CAOS (Payne et al., 2021) require as input temporal changes in sea ice concentration, atmospheric conditions (e.g., 10 m wind, air temperature, pressure, relative humidity, and cloud cover), albedo, idealized temperature and salinity profiles, and cloud-adjusted surface irradiance (Dobson & Smith, 1988; Gregg & Carder, 1990). GOTM produces hourly profiles of temperature, salinity, buoyancy frequency, and turbulent diffusion coefficients, while CAOS dynamically simulates the vertical behavior of N-based state variables, including sea ice algae, small and large phytoplankton, small and large zooplankton, nitrate (NO_3^-), ammonium (NH_4^+), and detritus. The sediment model, OMEXDIA (Soetaert et al., 1996a, 1996b), requires input of bottom-water concentrations of NO_3^- and NH_4^+ and

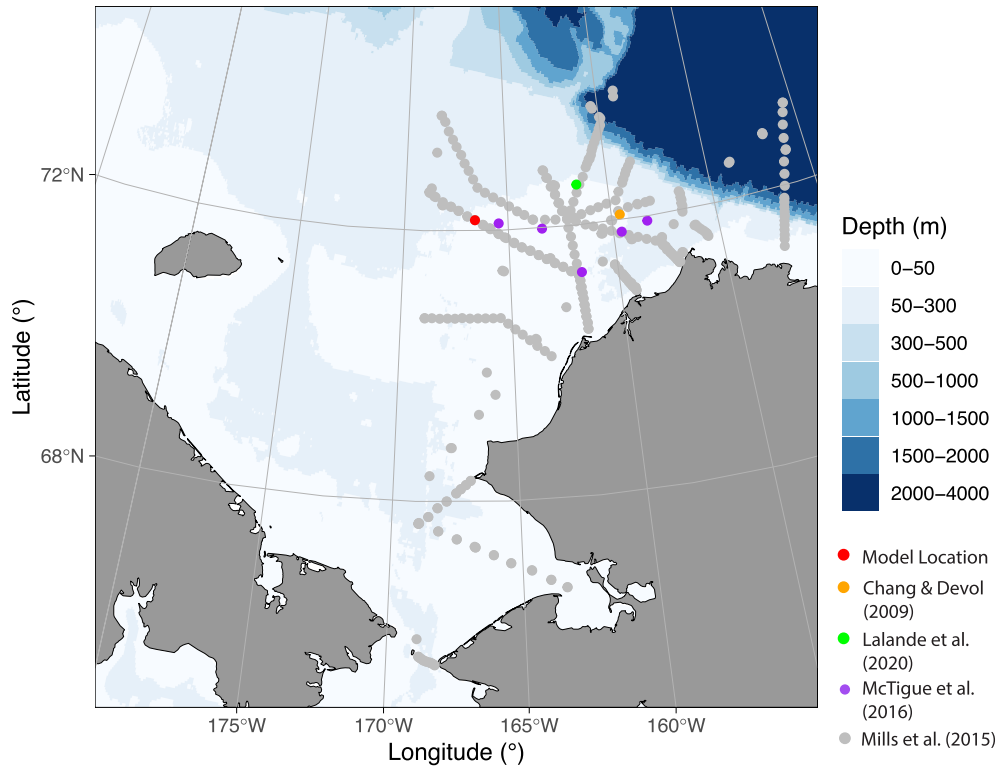

Figure 2. Bathymetric map of the Chukchi sea. Points represent the location of the model (red) in relationship to observational data collected by Chang and Devol (2009; orange), Lalande et al. (2020; green), McTigue et al. (2016; purple), and Mills et al. (2015; gray).

rates of PON export to the benthos from CAOS, as well as bottom-water temperature and salinity from GOTM. OMEXDIA simulates daily changes in fast- and slow-remineralizing organic matter, oxygen (O_2), NO_3^-, NH_4^+, N_2, and a reduced substances state variable. OMEXDIA also calculates rates of oxic and anoxic remineralization (where PON is converted to NH_4^+), nitrification, and denitrification, as well as vertical fluxes of NO_3^- and NH_4^+ between the sediments and the water column which are subsequently used by CAOS. While Soetaert et al. (1996b) use ammonia (NH_3) to represent the combined pools of NH_4^+ and NH_3, here we will use the term NH_4^+ throughout because this molecule is dominant at the typical ocean pH. Additionally, we report concentrations and rates taking place in thin layers in the sediments in nmol cm^{-3} but in mmol m^{-3} in the water column and for depth-integrated sedimentary processes (units are equivalent). For more complete model details, see Payne et al. (2021).

Satellite-derived and reanalysis data were used as inputs for CAOS-GO. Atmospheric conditions were determined using the National Centers for Environmental Prediction (NCEP) North American Regional Reanalysis (NARR; 32 km resolution used in this model configuration) products, which were provided by NOAA/OAR/ESRL PSL, Boulder, Colorado, USA from their website at https://psl.noaa.gov/data/gridded/. Idealized temperature profiles used in GOTM were determined using NOAA OISST version 2.1 (0.25° latitude and longitude resolution) data (Reynolds et al., 2007), provided by the NOAA/OAR/ESRL PSL, Boulder, Colorado, USA, from their website at https://psl.noaa.gov/. The mean of two Arctic Ocean snow depth models, SnowModel-LG (Liston et al., 2020; Stroeve et al., 2020, 25 km resolution) and CPOM (Zhou et al., 2021, 12.5 km resolution), was used to compute snow and melt pond thicknesses. Ice age (Tschudi et al., 2019, 62.5 km resolution used here) was used to calculate sea ice thickness and melt pond areal coverage (Webster et al., 2015). The National Snow and Ice Data Center (NSIDC) snow melt onset date (Anderson et al., 2019, 75 km resolution) provided the start date of snow melt each year. Sea ice began melting (and melt ponds began to form) on the first day when daily average NCEP NARR 2 m air temperature rose above 0°C at the model location. The timing of sea ice retreat and advance were set using sea ice concentration data (75 km resolution used here), provided by the NOAA/NSIDC Climate Data Record mean sea ice concentration (Meier et al., 2019; Peng et al., 2013). See Supporting Information S1 for methods and results of sensitivity analyses.

2.2. Under-Ice, Marginal Ice Zone, and Open Water Periods

As in Payne et al. (2021), we divided the annual cycle into the UI, marginal ice zone (MIZ), and open water (OW) periods. The UI bloom period extended from the initiation of exponential phytoplankton growth (when phytoplankton N assimilation exceeded 0.5 mmol m^{-2} d^{-1}) and lasted until the start of sea ice retreat, when satellite-derived sea ice concentration diminished below 90%. The MIZ period extended from the start of sea ice retreat until its conclusion, when sea ice concentrations diminished below 10%. Finally, the OW period began at the conclusion of ice retreat and terminated on the earliest date when either ice advanced in the autumn or light diminished below 1% the maximum value reached in the mixed layer, or on DOY 300 ± 6.

2.3. Winter Nitrate Inventory Experiment

Wintertime NO_3^- concentration shows minimal spatial variability across the Chukchi shelf; surface NO_3^- concentrations averaged 14.0 ± 1.91 mmol m^{-3} across the region in 2014 (Arrigo et al., 2017). To test the effect of pre-bloom winter NO_3^- concentration on rates of sedimentary denitrification, we ran the model for the year 2011, a year with a moderate UIB (Payne et al., 2021), under different initial (wintertime) NO_3^- conditions. To represent the range of wintertime NO_3^- concentrations observed in the Chukchi Sea (Mordy et al., 2020), we progressively altered the wintertime NO_3^- concentration by 2 mmol m^{-3} in a series of simulations, resulting in initial NO_3^- concentrations ranging from 10 to 26 mmol m^{-3} (or depth-integrated NO_3^- concentrations of 500–1300 mmol m^{-2}). These were used to test how much successive 100 mmol NO_3^- m^{-2} additions (2 mmol m^{-3} over 50 m) impacted N assimilation by microalgae, PON export to the benthos, nitrification, and denitrification at different initial NO_3^- concentrations.

2.4. Statistics

Multiple linear regressions were used to evaluate the importance of environmental conditions (e.g., ice thickness, length of UI period) on PON export to the sediments and denitrification rates. First, we checked for collinearity by using the variance inflation factor (VIF). Variables were only moderately correlated (VIF was <3 for all variables) and should have minimal impact on the correlations. Multiple linear regression variables were identified using backward selection, whereby the variable with the highest p-value was sequentially eliminated until only statistically significant variables ($p < 0.05$) remained. These regressions were subsequently checked using the Shapiro-Wilk test and visual inspection of histograms, quantile-quantile plots, and plots of the independent and dependent variables. Linear regressions are reported with the standard error, and plots with linear regressions include a confidence interval of 95%.

To cluster annual cycles of daily NPP into distinct types, *k*-means clustering was used based on NPP in the UI and MIZ periods. The gap statistic was used to determine the optimal *k* value. The annual cycle of N assimilation by microalgae each year was separated into one of three different temporal patterns based on the relative amount of assimilation during the UI and MIZ periods: years dominated by blooms in the UI period (17 of 31 years), years dominated by blooms in the MIZ period (4 of 31 years), or mixed years when both the UI and MIZ blooms were approximately equal (10 of 31 years; Table 1). To quantify the relationship between annual nitrification and denitrification rates and the annual bloom type, ANOVA and post hoc Tukey's honest significant difference tests were used. All statistical analyses were conducted in R version 4.1.0, including the relative importance of each variable in multiple linear regressions, which was assessed using the relaimpo package version 2.2–6 (Grömping, 2006).

3. Results

3.1. Annual Cycles in Sedimentary Processes

As water column NPP increased in the spring, particle export to the benthos increased shortly afterward, subsequently leading to changes in sedimentary processes. For example, in 2011, a year with a moderate UIB (Table 1; Payne et al., 2021), the phytoplankton bloom began on DOY 113 and peaked during the UI period (on DOY 147) at 352.0 mmol m^{-2}. Particulate organic N export to the benthos peaked eight days later (on DOY 155; Figure 3b) at 6.5 mmol m^{-2} d^{-1}. Particulate organic N export to the benthos diminished below 0.1 mmol m^{-2} d^{-1} on DOY 326, when N assimilation by microalgae was 0.1 mmol m^{-2} d^{-1}.

Table 1
Modeled Dominant Bloom Type (Under-Ice (UI)-Dominant, Marginal Ice Zone (MIZ)-Dominant, or Mixed (Mix) Dominance), Winter Ice Thickness (m), Winter Snow Thickness (m), Length of the UI Period (d), Length of the MIZ Period (d), Length of the Open Water (OW) Period (d), Annual N Assimilation (Assim.; mmol m^{-2} yr^{-1}), Benthic Particulate Organic N Export (mmol m^{-2} yr^{-1}), Water Column Nitrification (W.C. Nitr.; mmol m^{-2} yr^{-1}), Sedimentary Nitrification (S. Nitr.; mmol N m^{-2} yr^{-1}), and Sedimentary Denitrification (S. Denit.; mmol m^{-2} yr^{-1}) for each year from 1988 to 2018

Year	Dominant bloom	Winter ice thick.	Winter snow thick.	UI period	MIZ period	OW period	N assim.	PON export	W.C. nitr.	S. nitr.	S. denit.
1988	Mix	2.0	0.17	36	98	0	850.4	240.0	464.9	146.5	168.0
1989	UI	1.8	0.22	54	27	94	1012	313.4	456.5	185.0	227.3
1990	Mix	2.4	0.15	41	22	116	915.5	259.8	496.3	173.3	196.5
1991	Mix	2.6	0.16	49	45	87	840.1	229.4	466.7	143.3	152.2
1992	Mix	2.5	0.13	44	27	99	832.6	227.3	451.9	147.4	160.8
1993	MIZ	2.4	0.21	22	33	118	996.2	299.2	479.6	176.5	210.3
1994	UI	1.7	0.06	91	26	50	1050	331.7	464.0	199.8	249.7
1995	UI	2.2	0.21	61	42	91	1065	340.0	495.8	204.4	249.9
1996	UI	1.5	0.09	66	28	134	1116	366.4	493.0	226.8	284.6
1997	UI	1.6	0.13	39	23	141	963.0	288.1	466.3	180.8	220.6
1998	MIZ	2.6	0.13	13	35	122	960.5	282.1	466.1	173.3	205.5
1999	Mix	2.5	0.19	33	23	86	972.1	285.9	504.6	175.5	201.5
2000	Mix	2.5	0.14	37	43	51	863.1	240.0	462.8	157.3	177.0
2001	UI	1.7	0.10	38	25	73	946.1	279.9	464.4	178.2	214.1
2002	UI	1.8	0.11	68	9	106	1077	343.3	474.4	202.4	250.6
2003	UI	1.6	0.10	64	36	111	1065	338.0	479.9	202.9	253.2
2004	MIZ	2.5	0.05	20	43	121	936.7	272.0	464.4	177.5	210.0
2005	Mix	2.3	0.10	39	25	123	956.8	274.6	497.9	175.8	201.5
2006	UI	2.5	0.19	59	21	129	954.6	280.8	492.7	170.8	200.6
2007	UI	1.5	0.08	67	21	150	1084	343.6	501.1	208.0	258.1
2008	UI	1.5	0.11	61	24	109	1039	328.1	457.3	203.4	252.1
2009	UI	1.5	0.18	61	28	114	1104	367.4	450.3	211.0	270.6
2010	MIZ	2.5	0.14	6	41	133	912.8	260.8	444.8	176.2	207.0
2011	UI	1.5	0.17	55	22	140	1099	356.2	483.9	212.1	264.2
2012	Mix	2.3	0.15	38	36	92	904.9	259.7	487.1	168.7	195.0
2013	UI	1.6	0.08	78	21	121	1111	363.0	488.5	213.1	266.6
2014	Mix	2.6	0.13	43	38	110	915.5	260.9	504.8	178.1	199.9
2015	UI	1.7	0.06	62	25	129	1086	345.9	510.1	199.7	246.7
2016	Mix	2.3	0.09	40	22	162	929.6	267.8	499.8	180.0	207.4
2017	UI	1.4	0.09	47	27	170	1087	343.3	535.7	209.7	256.1
2018	UI	1.5	0.07	56	33	149	1102	355.4	521.8	221.5	272.6

As PON was exported to the benthos, sedimentary concentrations of O_2, NO_3^-, and NH_4^+ underwent rapid changes. O_2, which maintained a concentration of 300 nmol cm^{-3} in the top 0.01 mm of the sediments, dropped to near-zero below the top 3 mm (Figure 3c). Within 6 days of the peak in deposition of PON to the sediments (DOY 161), oxic remineralization and, to a lesser extent, nitrification and the oxidation of reduced substances, drove down the O_2 concentration to ≤1 nmol cm^{-3} below the top 0.3 mm of the sediments. Oxic remineralization (Figure 3f) peaked at the surface of the sediments at a rate of 15,000 nmol cm^{-2} d^{-1}. The oxic remineralization of organic N generates NH_4^+, the depth-integrated concentrations of which peaked 12 days after the peak in PON export (DOY 167), with concentrations increasing to 55 nmol cm^{-3} over the top 5 mm of the sediments (Figure 3e). Two other processes, anoxic remineralization and nitrification, both peaked at this same time (DOY 167).

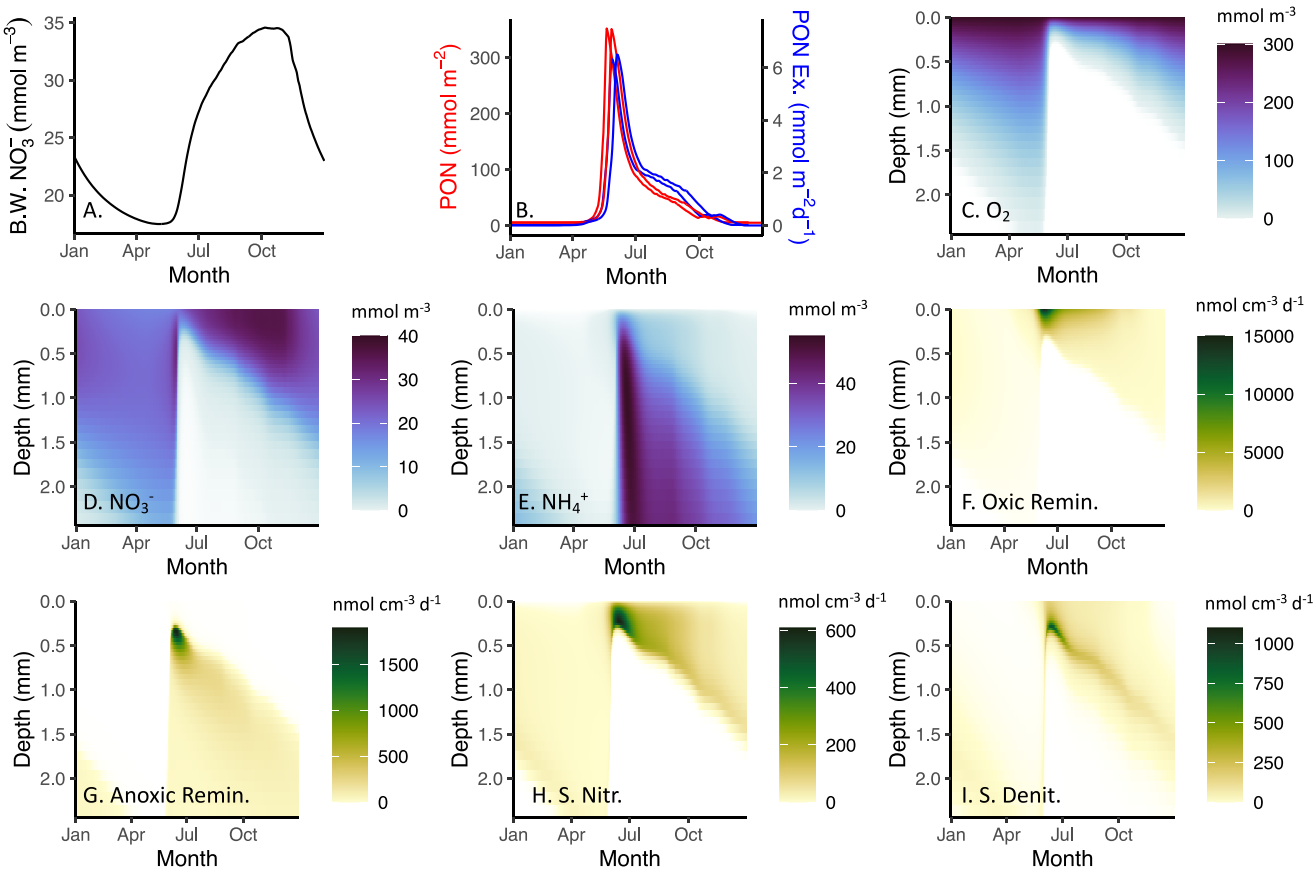

Figure 3. Modeled annual cycles of state variables for the standard run year, 2011. (a) Bottom-water NO_3^- concentration (mmol m^{-3}), (b) depth-integrated phytoplankton particulate organic nitrogen (PON; mmol m^{-2}; red) and PON exported to the sediments (mmol m^{-2} d^{-1}; blue), and (c) O_2 (mmol m^{-3}), (d) NO_3^- (mmol m^{-3}), (e) NH_4^+ (mmol m^{-3}), (f) oxic remineralization (nmol cm^{-3} d^{-1}), (g) anoxic remineralization (nmol cm^{-3} d^{-1}), (h) sedimentary nitrification (nmol cm^{-3} d^{-1}), and (i) sedimentary denitrification (nmol cm^{-3} d^{-1}) for the top 2.5 mm of the sediments.

Anoxic remineralization (Figure 3g) is inhibited by both O_2 and NO_3^- concentrations (such that concentrations of 1 nmol cm^{-3} of either substance reduces anoxic remineralization by 50%) and peaked at a rate of 1890 nmol cm^{-2} d^{-1} at a depth of 0.4 mm on DOY 165. Nitrification (Figure 3h), the process by which NH_4^+ is oxidized to NO_3^-, peaked at a rate of 600 nmol cm^{-2} d^{-1} on DOY 165 in the top 0.2 mm. Because O_2 concentrations diminished as nitrification rates increased and because high bottom-water NO_3^- concentrations drove diffusion into the sediments, almost all NO_3^- produced through sedimentary nitrification was subsequently denitrified. As a result, sedimentary NO_3^- concentrations diminished (Figure 3d), reaching their lowest concentration on DOY 163, as nitrification intensified, driving higher diffusion of NO_3^- into the sediments. Denitrification (Figure 3i) dominated in a very thin layer at a depth of 0.3 mm and peaked on DOY 166, one day after the peaks in anoxic remineralization and nitrification and 11 days after the maximal PON export to the benthos.

In the months following the peak in PON export to the benthos, concentrations of O_2 and NO_3^- gradually increased at depths between 0.3 and 3 mm in the sediments, while NH_4^+ concentrations diminished over this same period. As a result, processes that were highly concentrated in the top 0.4 mm of the sediments during peak PON export to the benthos happened over a more diffuse layer of the sediments (the top ~3 mm) in the autumn and winter. As expected, oxic processes (oxic remineralization and nitrification) closely resembled the distribution of O_2 (and thus NO_3^-) in the sediments throughout the year, while anoxic processes (anoxic remineralization and denitrification) were inversely related to O_2 concentration (and thus the distribution of NH_4^+).

3.2. Interannual Variance in Phytoplankton Bloom Timing and PON Export to the Benthos

Between 1988 and 2018, the phytoplankton bloom began on average in mid-May (DOY 137 ± 21), shifting earlier by 1.1 d each year ($R^2 = 0.238$, $p = 0.005$). Biomass typically peaked in mid-June during the UI period (8.4 ± 17.4 days prior to the start of ice retreat, or on DOY 170 ± 20), and this peak shifted earlier by 1.0 d yr^{-1} ($R^2 = 0.187$, $p = 0.015$) between 1988 and 2018. Blooms peaked at a concentration of 292.6 ± 57.4 mmol m^{-2} and daily N assimilation by microalgae (phytoplankton and sea ice algae) peaked at 54.9 ± 16.5 mmol m^{-2} d^{-1}, eventually dropping below 0.5 mmol m^{-2} d^{-1} on DOY 294 ± 13. Particulate organic N export to the benthos increased above 0.1 mmol m^{-2} d^{-1} on DOY 135 ± 27 and the onset of PON export shifted earlier by 1.3 d y^{-1} ($R^2 = 0.183$, $p = 0.016$). Particle export peaked on average at a rate of 5.1 ± 1.3 mmol m^{-2} d^{-1} on DOY 181 ± 23. Particulate organic N export diminished below 0.1 mmol m^{-2} d^{-1} on average on DOY 321 ± 11.

There was substantial interannual variability in the annual magnitude of PON exported to the benthos, which ranged from 227.3 to 367.4 mmol m^{-2} yr^{-1} between 1988 and 2018 (mean = 301.4 ± 44.5 mmol m^{-2} yr^{-1}; Figure 4a), increasing annually by 1.8 ± 0.8 mmol m^{-2} yr^{-1} ($R^2 = 0.130$, $p = 0.047$; Figure 4a). Annual PON export averaged 30.2 ± 1.8% of the magnitude of annual N assimilation by microalgae, or 46.0 ± 3.6% of annual NO_3^- assimilation. The annual peak in daily PON export ranged from 2.9 in 1991 to 6.9 mmol m^{-2} d^{-1} in 2009 (mean = 5.1 ± 1.3 mmol m^{-2} d^{-1}; Figure 5a). Multiple linear regression revealed that 76.5% of the variance ($p < 0.001$) in annual PON export to the benthos was controlled by a combination of sea ice thickness ($R^2 = 0.419$, $p < 0.001$), the length of the UI period ($R^2 = 0.229$, $p = 0.025$), and the length of the OW period ($R^2 = 0.117$, $p = 0.006$). These same three factors were most influential in determining the amount of N assimilated by microalgae each year, explaining 75.2% of the variance ($p < 0.001$) in annual N assimilation. Indeed, PON export to the sediments was highly correlated with annual N assimilation by microalgae, which explained 99.1% of the variance in PON export ($p < 0.001$, slope = 0.538, Figure 4b). Variation in N assimilation by UI microalgae accounted for 47.8% of the variance ($p < 0.001$) in annual PON export, which is substantially more than that explained by N assimilation during the MIZ ($R^2 = 0.295$, $p = 0.002$) or OW (not statistically significant) periods.

The timing of PON export to the benthos also changed between 1988 and 2018 (Figure 5a). Organic matter exported to the sediments peaked between 6 and 36 days after the peak in phytoplankton biomass (mean = 11.2 ± 7.8 after the biomass peak, or on DOY 181 ± 23) with the peak coming earlier by 1.2 d yr^{-1} ($R^2 = 0.200$, $p = 0.012$; Figure 5a). Additionally, PON export increased significantly between 1988 and 2018 in the months of March-June (Table 2, Figure 5a), but showed no significant trends in other months.

3.3. Nitrification and Denitrification

Daily water column nitrification rates ranged between a minimum of 0.01 ± 0.004 mmol m^{-2} d^{-1} and an average peak of 8.3 ± 1.3 mmol m^{-2} d^{-1} (Figure 5b) between 1988 and 2018. Water column nitrification rates typically peaked on DOY 177.5 ± 18.9, and this peak shifted earlier by 0.9 d yr^{-1} between 1988 and 2018 ($R^2 = 0.204$, $p = 0.011$). Annual depth-integrated water column nitrification rates ranged from 444.8 to 535.7 mmol m^{-2} yr^{-1} (mean = 481.5 ± 22.3 mmol m^{-2} yr^{-1}; Figure 4c), equivalent to 48.9 ± 4.2% of annual N assimilation by microalgae. The annual rate of water-column nitrification increased by 1.2 ± 0.4 mmol m^{-2} yr^{-1} ($R^2 = 0.239$, $p = 0.005$) between 1988 and 2018. Annual water-column nitrification was weakly but significantly correlated with annual N assimilation by microalgae ($R^2 = 0.135$, $p = 0.042$; Figure 4d). Multiple linear regression revealed that 29.2% of the variance ($p < 0.001$) in annual water column nitrification was controlled by the length of the snow melt period. Because N assimilation by microalgae during the OW period was concentrated at the depth of the subsurface Chl *a* maximum (Payne et al., 2021) and water-column nitrification rate increased with depth in the CAOS model, variation in OW N assimilation accounted for 28.5% of the variance in water column nitrification ($p = 0.002$), while variation in UI and MIZ N assimilation showed no statistically significant relationship with water column nitrification.

Daily sedimentary nitrification rates ranged from a minimum of 0.19 ± 0.03 mmol m^{-2} d^{-1} to a mean peak daily rate of 1.1 ± 0.1 mmol m^{-2} d^{-1} (Figure 5c). Annual sedimentary nitrification rates were much lower than those in the water column, ranging from 143.3 to 226.8 mmol m^{-2} yr^{-1} (mean = 186.4 ± 22.2 mmol m^{-2} yr^{-1}; Figure 4e) and nitrifying on average 18.8 ± 0.8% of annual N assimilated by microalgae and 62.1 ± 3.0% of exported PON. Similar to water column nitrification, annual sedimentary nitrification increased by 1.1 ± 0.4 mmol m^{-2} yr^{-1} each year between 1988 and 2018 ($R^2 = 0.220$, $p = 0.008$). Multiple linear regression revealed that 77.7% of the

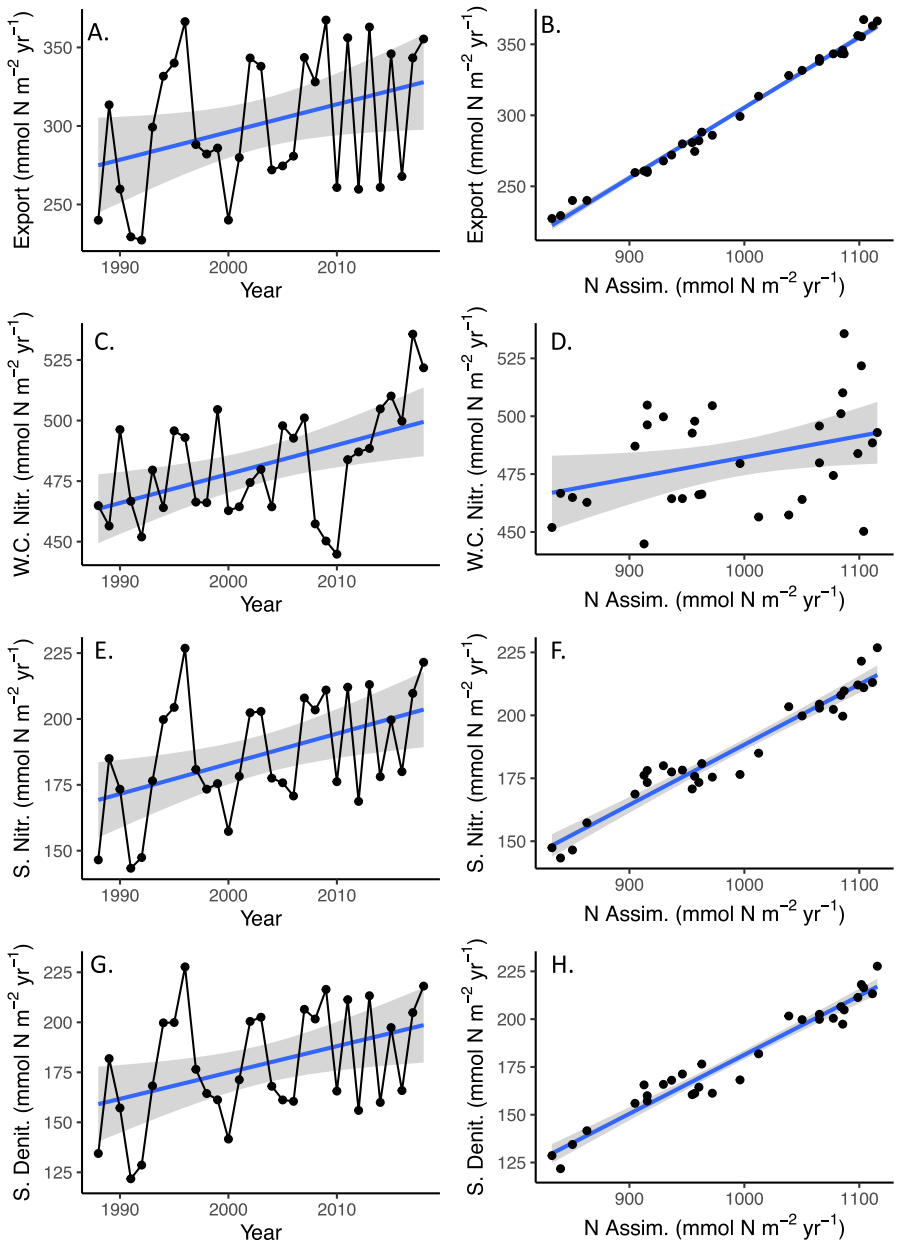

Figure 4. Modeled interannual trends for 1988–2018 in (a) particulate organic nitrogen (PON) export to the benthos (mmol m^{-2} yr^{-1}), (c) water column (W.C.) nitrification (mmol m^{-2} yr^{-1}), (e) sedimentary nitrification (mmol m^{-2} yr^{-1}), and (g) sedimentary denitrification (mmol m^{-2} yr^{-1}). Scatterplots of annual N assimilation (Assim.) versus (b) PON export to the benthos (mmol m^{-2} yr^{-1}), (d) W.C. nitrification (mmol m^{-2} yr^{-1}), (f) sedimentary nitrification (mmol m^{-2} yr^{-1}), and (h) sedimentary denitrification (mmol m^{-2} yr^{-1}). Blue line indicates statistically significant linear regressions and gray shading represents the 95% confidence interval for these regressions.

variance ($p < 0.001$) in annual sedimentary nitrification was controlled by a combination of sea ice thickness ($R^2 = 0.388$, $p < 0.001$), the length of the OW period ($R^2 = 0.200$, $p < 0.001$), and the length of the UI period ($R^2 = 0.189$, $p = 0.041$). Annual N assimilation by microalgae was highly correlated with annual sedimentary nitrification, explaining 93.1% of the interannual variance ($p < 0.001$; Figure 4f). Variation in N assimilation by microalgae during the UI period drove more of the variance in annual sedimentary nitrification (40.0%) than the other two periods ($p < 0.001$).

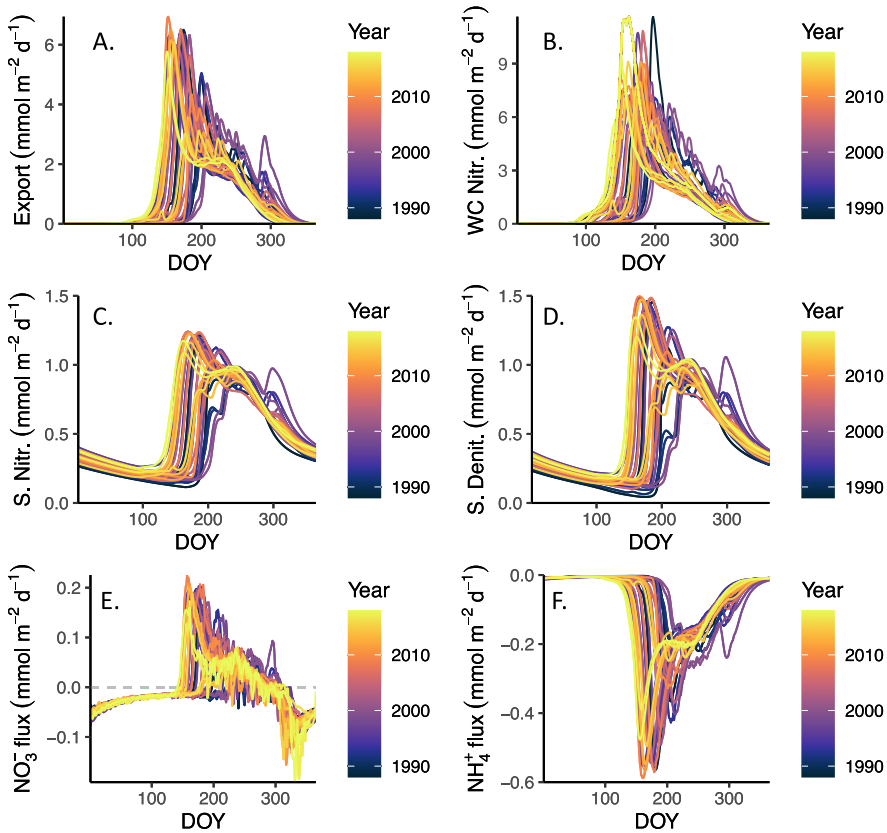

Figure 5. Modeled interannual differences in (a) particulate organic nitrogen (N) export to the benthos (mmol m^{-2} d^{-1}), (b) water column nitrification (mmol m^{-2} d^{-1}), (c) sedimentary nitrification (mmol m^{-2} d^{-1}), (d) sedimentary denitrification (mmol m^{-2} yr^{-1}), (e) NO_3^- flux into the sediments (mmol m^{-2} yr^{-1}), and (f) NH_4^+ flux into the sediments (mmol m^{-2} yr^{-1}) for each day of the year (DOY) between 1988 and 2018 (colorbar). The year 1999 (purple) had a large autumn bloom following a mixing event in early October and this increase in N assimilation subsequently drove an anomalous spike in all other processes on DOY ~300.

Because of high water column O_2 concentrations, denitrification was limited to the sediments. Average daily denitrification rates ranged from 0.14 ± 0.04 to 1.2 ± 0.2 mmol m^{-2} d^{-1} (Figure 5d), while annual denitrification ranged from 121.8 to 227.7 mmol m^{-2} yr^{-1} between 1988 and 2018 (mean = 178.8 ± 28.3 mmol m^{-2} yr^{-1}; Figure 4g). Sedimentary denitrification removed a mean of 17.9 ± 1.4% of the annual N assimilated by microalgae, 59.3 ± 2.3% of the PON exported to the sediments, and 95.5 ± 4.3% of the NO_3^- produced through sedimentary nitrification. Annual denitrification increased annually over this period by 1.3 ± 0.5 mmol m^{-2} yr^{-1} ($R^2 = 0.179$, $p = 0.018$). Multiple linear regression revealed that 76.1% ($p < 0.001$) of the variance in annual denitrification was controlled by a combination of sea ice thickness ($R^2 = 0.616$, $p < 0.001$) and the length of the OW period ($R^2 = 0.145$, $p = 0.004$). Denitrification was highly correlated with both annual N assimilation by microalgae, which explained 94.9% of the variance in denitrification rates ($p < 0.001$; Figure 4h), and with PON export to the benthos, which explained 95.4% of the variance in denitrification ($p < 0.001$). Variation in N assimilation by microalgae during the UI period drove more of the variance in annual denitrification than the two other periods, accounting for 44.1% ($p < 0.001$).

Increases in annual rates of nitrification and denitrification between 1988 and 2018 were driven by increases in these processes between January and June (Figures 5b–5d). Water-column nitrification increased significantly in February-June while sedimentary nitrification increased in March-June (Table 2). Denitrification increased significantly over a longer time period, from January-June (Table 2).

Table 2
Modeled Linear Regressions of Time (1988–2018) Versus Monthly Benthic Particulate Organic N Export, Water Column Nitrification, Sedimentary Nitrification, and Sedimentary Denitrification (Units of mmol m^{-2} per Month yr^{-1})

Process	Month	R^2	*p*-value	Slope
Benthic export	March	0.132	0.045	9.82E−4
Benthic export	April	0.245	0.005	1.36E−3
Benthic export	May	0.291	0.002	5.50E−3
Benthic export	June	0.167	0.022	1.73E−2
Water column nitrification	February	0.152	0.030	5.87E−5
Water column nitrification	March	0.255	0.004	1.24E−3
Water column nitrification	April	0.208	0.010	1.11E−2
Water column nitrification	May	0.243	0.005	6.77E−2
Water column nitrification	June	0.144	0.035	9.86E−2
Sedimentary nitrification	March	0.132	0.045	9.83E−4
Sedimentary nitrification	April	0.245	0.005	1.36E−3
Sedimentary nitrification	May	0.292	0.002	5.50E−3
Sedimentary nitrification	June	0.167	0.022	1.73E−2
Sedimentary denitrification	January	0.129	0.048	1.54E−3
Sedimentary denitrification	February	0.130	0.046	1.36E−3
Sedimentary denitrification	March	0.136	0.041	1.26E−3
Sedimentary denitrification	April	0.193	0.013	1.48E−3
Sedimentary denitrification	May	0.301	0.001	5.23E−3
Sedimentary denitrification	June	0.151	0.031	2.58E−2
NH_4^+ flux	April	0.215	0.009	−6.45E−3
NH_4^+ flux	May	0.240	0.005	−6.45E−1

Note. R^2, *p*-value, and slope is listed for each statistically significant ($p < 0.05$) month.

3.4. Sediment-Water Exchange of NO_3^- and NH_2^+

NO_3^- and NH_4^+ fluxes across the sediment-water interface in the OMEX-DIA model vary depending on the bottom-water salinity, temperature, and NO_3^- and NH_4^+ concentrations (Soetaert et al., 1996a, 1996b). The sediments were typically a net source of NO_3^- to the overlying water column, supplying 2.3 ± 1.9 mmol m^{-2} yr^{-1}. NO_3^- diffused out of the sediments in the early part of the year at a rate of 0.05 mmol m^{-2} d^{-1} due to lower NO_3^- concentrations in the water column. However, this pattern reversed on DOY 176 ± 24 when NO_3^- began to diffuse into the sediments, peaking on DOY 199 ± 36 at a rate of 0.14 ± 0.06 mmol m^{-2} d^{-1} (Figure 5e). In autumn, the sediments once again became a net source of NO_3^- to the water column, peaking at a rate of 0.10 ± 0.03 mmol m^{-2} d^{-1} on DOY 319 ± 60. While there was no secular trend in either the annual net NO_3^- flux from the sediments to the water column, the peak timing, or the peak magnitude, there was a slight increase in the magnitude in the peak flux rate of NO_3^- out of the sediments in the autumn between 1988 and 2018 ($R^2 = 0.243$, $p = 0.005$, slope = −0.002).

In contrast to the sediment-water flux of NO_3^-, which could represent either a source to or sink of water-column NO_3^-, the sediments consistently acted as a source of NH_4^+ to the water column at an average rate of 29.8 ± 5.1 mmol m^{-2} yr^{-1}. In general, the supply of NH_4^+ to the water column peaked at a rate of 0.42 ± 0.13 mmol m^{-2} d^{-1} on DOY 190 ± 24 (Figure 5f). While the magnitude of the peak NH_4^+ flux did not change over time, the peak shifted earlier by 1.1 d yr^{-1} ($R^2 = 0.180$, $p = 0.018$) from 1988 to 2018.

3.5. Water Column Bloom Types

Of the 31 years between 1988 and 2018, 17 years were dominated by NPP in the UI period, 4 by NPP in the MIZ period, and 10 featured a mix of both UI and MIZ blooms (Table 1). Years when UI blooms were dominant had higher annual N assimilation by microalgae (1056.5 ± 55.5 mmol m^{-2} yr^{-1}) than either MIZ-dominant (951.6 ± 35.6 mmol m^{-2} yr^{-1}, $p = 0.003$) or mixed-dominance (898.1 ± 49.1 mmol m^{-2} yr^{-1}, $p < 0.001$) years. In years with high N assimilation by microalgae in the UI period, PON export to the benthos (334.4 ± 28.2 mmol m^{-2} yr^{-1}) was also greater than in years with either MIZ (278.5 ± 16.3 mmol m^{-2} yr^{-1}, $p < 0.001$) or mixed-dominance blooms (254.5 ± 19.6 mmol m^{-3} yr^{-1}, $p < 0.001$). While nitrification in the water column showed no significant differences with bloom type, there were significant differences in sedimentary nitrification, with UI-dominant years having higher rates of sedimentary nitrification (201.7 ± 15.2 mmol m^{-2} yr^{-1}) than either mixed-dominance years (164.6 ± 14.5 mmol m^{-2} yr^{-1}, $p < 0.001$) or MIZ-dominant years (175.9 ± 1.8 mmol m^{-2} yr^{-1}, $p = 0.007$). As a result, UI-dominant years also had higher sedimentary denitrification rates (199.4 ± 17.7 mmol m^{-2} yr^{-1}) than either mixed-dominance years (148.8 ± 15.8 mmol m^{-2} yr^{-1}, $p < 0.001$) or MIZ-dominant years (166.6 ± 1.9 mmol m^{-2} yr^{-1}, $p < 0.003$).

3.6. Sensitivity to Initial NO_3^- Concentration

To test how a change in the wintertime NO_3^- concentration (which might be caused by a change in advection from the Bering to the Chukchi Sea) could impact water column and sedimentary N biogeochemistry, we increased initial wintertime NO_3^- concentration in successive runs by 100 mmol m^{-2} (2 mmol m^{-3} over the 50 m water column), resulting in final concentrations ranging from 600 to 1300 mmol m^{-2} (12–26 mmol m^{-3}; Table 3). Results indicate that the N cycle in the Chukchi Sea is quite sensitive to the addition of new NO_3^- to the system, with most (79%–86%) of the incremental 100 mmol m^{-2} NO_3^- additions being assimilated by phytoplankton by the end of the year (Table 3). Most of this increase is driven by higher NO_3^- assimilation during the UI period

Table 3
The Impact of a 100 mmol m^{-2} Increase in Modeled Wintertime NO_3^- Concentration at a Variety of Initial NO_3^- Concentrations (With Final Concentrations Changing From 12 to 26 mmol m^{-3}, or 600–1300 mmol m^{-2}) on total annual N assimilation (mmol m^{-2} yr^{-1}); N assimilation during the UI, MIZ, and OW periods (mmol m^{-2} yr^{-1}); PON export to the benthos (mmol m^{-2} yr^{-1}); mean water-column NO_3^- concentration (mmol m^{-2}); water-column nitrification (W.C. Nitr.; mmol m^{-2} yr^{-1}); sedimentary nitrification (S. Nitr.; mmol m^{-2} yr^{-1}); sedimentary denitrification (S. Denit.; mmol m^{-2} yr^{-1}); and NO_3^- and NH_4^+ fluxes across the sediment-water interface (mmol m^{-2} yr^{-1})

Range Init. NO_3^-	Δ Init. NO_3^-	Δ NO_3^- assim.	Δ UI NO_3^- assim.	Δ MIZ NO_3^- assim.	Δ OW NO_3^- assim.	Δ N export	Mean Δ NO_3^-	Δ W.C. nitr.	Δ S. nitr.	Δ S. denit.	Δ NO_3^- flux	Δ NH_4^+ flux
500–600	100	85.8	65.5	−0.9	21.1	34.4	81.8	54.3	14.2	25.6	−3.3	4.7
600–700	100	83.2	65.3	−1.2	19.2	32.4	82.9	53.9	13.0	31.8	−3.4	4.8
700–800	100	83.2	65.6	−0.8	18.4	31.1	83.5	54.8	11.5	30.8	−3.6	4.9
800–900	100	81.7	65.7	−1.2	17.2	29.9	84.0	54.5	10.3	30.1	−3.8	4.9
900–1000	100	81.6	65.6	−0.2	16.2	28.4	84.8	55.6	9.2	29.3	−3.9	4.8
1000–1100	100	82.1	64.8	0.0	17.2	27.7	85.4	56.6	8.6	29.2	−4.1	4.8
1100–1200	100	79.1	60.4	1.3	17.5	24.5	86.7	57.0	7.4	27.5	−4.0	4.3
1200–1300	100	79.2	60.5	1.2	17.6	23.8	87.0	57.5	6.9	27.4	−4.1	4.3

(61–66 mmol m^{-2} yr^{-1}), with a sizable proportion also assimilated during the OW period (17–21 mmol m^{-2} yr^{-1}). Almost none of the added NO_3^- was assimilated within the MIZ.

This 79–86 mmol m^{-2} yr^{-1} increase in N assimilation by phytoplankton in response to a 100 mmol m^{-2} incremental increase in wintertime NO_3^- translated to a 24–34 mmol m^{-2} yr^{-1} increase in PON export (Table 3). As a result, rates of nitrification in the water column and the sediments increased by 54–58 and 7–14 mmol m^{-2} yr^{-1}, respectively, and the sedimentary denitrification rate increased by 26–32 mmol m^{-2} yr^{-1}. Finally, each 100 mmol m^{-2} increase in wintertime NO_3^- decreased the NO_3^- flux out of the sediments by 3–4 mmol m^{-2} yr^{-1} and increased the flux of NH_4^+ by 4–5 mmol m^{-2} yr^{-1}.

Interestingly, as initial NO_3^- concentration was increased from 600 to 1300 mmol m^{-2}, each incremental 100 mmol m^{-2} increase in water column NO_3^- had a diminishing effect on many N-cycle processes such as NO_3^- assimilation, PON export to the benthos, sedimentary nitrification, and NH_4^+ flux out of the sediments (Table 3). Conversely, the same 100 mmol m^{-2} increase in water column NO_3^- enhanced the mean water-column NO_3^- concencentration, water-column nitrification, sedimentary denitrification, and NO_3^- flux from the sediments (Table 3).

4. Discussion

The Chukchi Sea accounts for 0.2% of global ocean surface area but 1%–3% of global fixed N loss in the oceans (Chang & Devol, 2009) due to the coupled partial nitrification-denitrification processes that predominate in the shallow continental shelf sediments (Brown et al., 2015). Despite the outsized importance of this region to global fixed N loss, field measurements of denitrification rates in the Chukchi Sea are sparse and largely confined to areas near the shelf break in the northeastern Chukchi Sea (see Figure 2). Measured rates of sedimentary denitrification on the 50 m deep continental shelf of the northern Chukchi Sea ranged from 0.76 to 1.58 mmol m^{-2} d^{-1} in the summer of 2004 (Chang & Devol, 2009) and from 0.14 to 0.98 mmol m^{-2} d^{-1} in August of 2013 (McTigue et al., 2016). The CAOS-GO model produced mean annual denitrification rates of 0.41–0.78 mmol m^{-2} d^{-1} and maximum rates of 0.82–1.50 mmol m^{-2} d^{-1} between 1988 and 2018. Rates of fixed N loss through denitrification have also been estimated from excess N measurements taken throughout the Chukchi Sea. Assuming non-Redfield uptake by phytoplankton, fixed N loss in the Chukchi Sea was calculated as 1.9 ± 2.3 and 4.1 ± 7.1 mmol m^{-3} in 2010 and 2011, respectively (Mills et al., 2015). CAOS-GO produced excess N in line with these values, ranging from 2.4 to 4.6 mmol m^{-3} between 1988 and 2018 (mean = 3.6 ± 0.6 mmol m^{-3}). Further, our results indicate that denitrification rates increased annually by 1.3 mmol m^{-2} yr^{-1} over this timeframe, indicating that the sediments of the northern Chukchi Sea may contribute even more to future N loss than previously calculated (Chang & Devol, 2009).

Much of this modeled increase in denitrification was attributable to the increase in annual NPP (Payne et al., 2021) and PON exported to the benthos. A 3.8 mmol m^{-2} yr^{-1} increase in N assimilation by microalgae between 1988 and 2018 corresponded to a 1.8 mmol m^{-2} yr^{-1} increase in PON export to the benthos. This trend was also observed in sediment traps deployed in the Hanna Shoal area by Lalande et al. (2020), who found that 2016 rates of Chl *a* export were substantially higher than previous measurements made in 2004 (Lalande et al., 2007). CAOS-GO produced a mean rate of POC export to the benthos of 29.2 ± 4.3 g C m^{-2} yr^{-1} between 1988 and 2018, comparable to the 29.7 g C m^{-2} yr^{-1} average export reported for the Chukchi Sea (Chang & Devol, 2009). A mooring deployed at 37 m depth (8 m above the seafloor) by Lalande et al. (2020) recorded a mean export rate of 3–5 mg Chl *a* m^{-2} d^{-1} from surface waters during a UIB in June-July 2016, similar to our modeled export rate for this same period of 3.0–4.8 mg Chl *a* m^{-2} d^{-1}.

The CAOS-GO model showed that particle export to the benthos and sedimentary nitrification and denitrification rates were all tightly coupled to the magnitude of annual NPP, which explained 93%–99% of the variance in these three rates. The high correlation between NPP and sedimentary processes is not surprising. For example, Townsend and Cammen (1988) argued that changes in the magnitude and seasonality of pelagic NPP directly affected the quantity and quality of the organic matter that arrives at the sediment surface, thus influencing benthic productivity. In the Arctic Ocean specifically, a study by Fu et al. (2016) used nine Earth system models to assess how climate change would impact Arctic NPP and export over time. These climate models projected that surface ocean-warming and freshening would result in an increase in stratification, leading to a reduction in nutrient inventories, which opposes most recent observations of nutrient inventories in the Arctic (Henley et al., 2020; Lewis et al., 2020; Mordy et al., 2020; Randelhoff et al., 2019, 2018). However, the models indicated that this decline in nutrient inventories would result in dininished NPP between the 1990s and 2090s and that this resulted in a decline in particle export to the benthos. The correlation between PON exported to the benthos and rates of coupled partial nitrification-denitrification in the sediments has similarly been widely observed (Baumann et al., 2013; Granger et al., 2011; Horak et al., 2013) and assumed in models (Chang & Devol, 2009; Fennel, 2010; Fennel et al., 2009; Laurent et al., 2016; Soetaert et al., 1996a, 1996b) used to calculate denitrification rates.

Sea ice algae and under-ice phytoplankton are considered to be efficient exporters of organic matter (Boetius et al., 2013; Fahl & Nöthig, 2007) because of their silicified cell walls (Smetacek, 1999) and because they face less grazing pressure than algae growing during warmer times of the year (Campbell et al., 2001; Conover & Huntley, 1991; Coyle et al., 2007; Huntley & Lopez, 1992). Indeed, previous work with the CAOS-GO model (Payne et al., 2021) demonstrated that zooplankton grazing was on average 3.5 times greater during the OW period than the UI period, even though the OW period generated only half the phytoplankton biomass. As a result of the reduced grazing pressure during the UI period, Arrigo et al. (2014) hypothesized that the massive UIBs observed in the northern Chukchi Sea would likely be disproportionately exported and might subsequently fuel increases in denitrification (Townsend & Cammen, 1988). This appears to be supported by CAOS-GO results, which indicate that secular increases in particulate export to the benthos and denitrification were driven by NPP generated early in the year (and thus mostly in the UI period) and by years where NPP was dominated by large UIBs.

However, the CAOS-GO model demonstrates that export efficiency is also closely tied to the depth over which phytoplankton production is generated. Ice algal and UI NPP modeled here were exported at a higher rate, but at a lower export efficiency, than NPP generated during the MIZ and OW periods when phytoplankton are concentrated within a subsurface Chl *a* maximum. This was because ice algal and UI blooms developed higher in the water column (at an average depth of 0 m and ∼15 m), and thus descended a longer distance and over a longer time period (at 5 m d^{-1}, or on average over 10 and 7 days, respectively) than MIZ and OW blooms (which were generated at a depth of 30 m on average and as a result sunk over 4 days). The longer period of sinking for ice algal and UI biomass allowed much more PON to be remineralized before reaching the sediments. At the 0.2 d^{-1} remineralization rate used in the CAOS-GO model, only 11% and 26% of the biomass produced in the ice algal and UI blooms, as compared to 41% of the MIZ/OW biomass, reached the sediments. Thus, the model indicates that the higher PON export and sedimentary denitrification rates associated with years with large UIBs is due to their higher annual NPP, rather than a greater export efficiency.

The secular increases in annual NPP, PON export to the benthos, and denitrification in the northern Chukchi Sea likely have large ramifications downstream. Satellite analysis of NPP in the Arctic Ocean (Arrigo & Van Dijken, 2015) revealed that an increase in Chukchi Sea NPP, likely driven by changing sea ice cover, was

followed by a significant decline in NPP in the Greenland Sea the following year. Arrigo and Van Dijken (2015) hypothesized that phytoplankton in the Chukchi Sea were able to consume a greater proportion of available NO_3^-, reducing NO_3^- availability and consequently NPP in the N-limited Greenland Sea (Krisch et al., 2020). Reductions in NPP in regions downstream of the Chukchi Sea could substantially limit food available to zooplankton, pelagic fish, marine mammals, and seabirds (Hamilton et al., 2021; Joiris, 2011; Munk, 2003; Rysgaard et al., 1999). Additionally, the Chukchi shelf has some of the lowest N* values (a measure of N excess relative to phosphorus; Gruber & Sarmiento, 1997) in the global ocean (Deutsch & Weber, 2012), driven by high sedimentary denitrification (Brown et al., 2015; Chang & Devol, 2009; Devol et al., 1997; Mills et al., 2015). A study by Yamamoto-Kawai et al. (2006) found that the excess phosphate relative to N in waters downstream of the Chukchi Sea stimulated N_2 fixation in the surface waters of the North Atlantic. Although N_2 fixation was previously considered only feasible in warm, N-deplete waters (Sohm et al., 2011), recent work has found ample evidence of both N_2 fixers (Blais et al., 2012; Díez et al., 2012; Fernández-Méndez et al., 2016; Moisander et al., 2010) and N_2 fixation (Baer et al., 2017; Blais et al., 2012; Mulholland et al., 2012; Sipler et al., 2017) in the Arctic Ocean. Higher rates of denitrification in the northern Chukchi Sea would further diminish the N* values of waters in the region, which in turn could spur an increase in N_2 fixation in both the Arctic (Tremblay & Gagnon, 2009) and the North Atlantic oceans (Yamamoto-Kawai et al., 2006). Rates of nitrogen fixation in the Arctic may already offset as much as 27% of the Arctic denitrification-driven N deficit (Sipler et al., 2017), further demonstrating the importance of this region in regulating the global N budget.

The CAOS-GO model showed secular increases in denitrification between 1988 and 2018 without any change in modeled N inventory. However, climate change has increased NO_3^- inventory in the Chukchi Sea through both the increase in advection of NO_3^--rich Pacific waters into the Arctic Ocean (Mordy et al., 2020; Peralta-Ferriz & Woodgate, 2017; Woodgate, 2018) and consequences of sea ice loss, including more frequent winter storms (Yang, 2004; Zhang et al., 2010), enhanced upwelling near shelf breaks (Carmack & Chapman, 2003; Tremblay et al., 2011; Tremblay & Gagnon, 2009), and the generation of internal waves (Rainville & Woodgate, 2009). Satellite analysis reveals that an increase in NO_3^- concentration and phytoplankton biomass has largely driven the increase in NPP in the Chukchi Sea since 2009 (Lewis et al., 2020). Our sensitivity analysis showed that by increasing the modeled wintertime NO_3^- concentration, 82% of the added NO_3^- was assimilated by phytoplankton, with most of this increase driven by assimilation during the UI period. However, NO_3^- additions also contributed to increases in particulate export to the benthos, sedimentary nitrification, and sedimentary denitrification; 30% of the added NO_3^- was subsequently exported to the benthos and lost through denitrification. As a result, CAOS-GO suggests that, while an increase in NO_3^- concentration will contribute to higher NPP both in the Chukchi Sea and in downstream ecosystems, one third of added N will subsequently be lost through coupled partial nitrification-denitrification in the northern Chukchi Sea.

The UI period can be critically important to the ecology and biogeochemistry of the northern Chukchi Sea. Our CAOS-GO model found that UIBs on average generated nearly 50% of annual NPP between 1988 and 2018 (Payne et al., 2021) and that the secular increase in NPP was driven largely by increases in the spring and thus largely during the UI period. Higher NPP subsequently led to increases in PON export to the benthos and sedimentary nitrification and denitrification. Thus, it appears that a period historically thought to support little phytoplankton growth (Hameedi, 1978; Perrette et al., 2011) is disproportionately important in the northern Chukchi Sea. In addition to impacting downstream regions (Arrigo & Van Dijken, 2015; Krisch et al., 2020; Tremblay & Gagnon, 2009; Yamamoto-Kawai et al., 2006), massive UIBs are altering northern Chukchi Sea ecosystems. By removing fixed N from the surface waters during a part of the year with low zooplankton growth (Sherr et al., 2008; Sherr et al., 2009), UIBs enhance the phytoplankton-zooplankton timing mismatch (Conover & Huntley, 1991). Our model demonstrates that years when production was dominated by UIBs featured 25% less zooplankton grazing than years with blooms only in the MIZ period (Payne et al., 2021) but that UI-dominant years have 15% more sedimentary nitrification and 20% more denitrification than MIZ-dominant years, indicating an increase in benthic-pelagic coupling. This likely negatively impacts the many fish, seabird, and marine mammal populations that rely on pelagic production in the northern Chukchi Sea (De Robertis et al., 2017; Kuletz et al., 2015; Logerwell et al., 2015; Moore & Kuletz, 2019). For example, fin whales, which time their migration to arrive as zooplankton abundance increases during the OW period (Tsujii et al., 2016), might encounter far fewer food sources in areas with large UIBs. While UIBs lead to reduced pelagic grazing, they could also substantially enhance benthic production (Townsend & Cammen, 1988) in a region that already supports rich benthic communities (Grebmeier, 2006; Grebmeier et al., 1988, 2015; Lalande et al., 2007). While our model did

not include changes in benthic macrofaunal communities, a field study by McTigue et al. (2016) indicates that high bioturbation and bioirrigation may enhance denitrification in the northern Chukchi Sea, indicating that our model results may even under-predict possible changes over time in sedimentary denitrification. However, our results should not be extrapolated across the Chukchi Sea or the Arctic Ocean as a whole. A remote sensing study estimating the frequency of MIZ and UI blooms in the Chukchi Sea by Lowry et al. (2014) seems to indicate that the southern Chukchi Sea experiences fewer MIZ blooms than the northern Chukchi Sea, and that UIBs are diminishing in spatial coverage over time. In contrast, a modeling study by Horvat et al. (2017) indicates that changing sea ice conditions is gradually making more regions of the Arctic Ocean amenable to UIB formation. Future studies (and especially field sampling campaigns) should investigate the spatial variability of UIBs as well as their biogeochemical and ecological ramifications.

Data Availability Statement

Model code and all data are available at https://purl.stanford.edu/gc896jc5127. Processed sediment model output and the raw output for the initial N experiments are available at https://purl.stanford.edu/xc612sy7581.

Acknowledgments
The authors would like to thank Gert van Dijken, Matthew Mills, Stephanie Lim, and Casey Schine for providing input on analysis.

References

Anderson, M., Bliss, A., & Drobot, S. (2019). Snow melt onset over arctic sea ice from SMMR and SSM/I-SSMIS brightness temperatures, version 3. NASA National Snow and Ice Data Center DAAC. https://doi.org/10.5067/A9YK15H5EBHK

Ardyna, M., Babin, M., Gosselin, M., Devred, E., Rainville, L., & Tremblay, J.-É. (2014). Recent Arctic Ocean sea ice loss triggers novel fall phytoplankton blooms. *Geophysical Research Letters*, *41*, 6207–6212. https://doi.org/10.1002/2014GL061047

Ardyna, M., Mundy, C. J., Mayot, N., Matthes, L. C., Oziel, L., Horvat, C., & Arrigo, K. R. (2020). Under-ice phytoplankton blooms: Shedding light on the "invisible" part of Arctic primary production. *Frontiers in Marine Science*, *7*, 608032. https://doi.org/10.3389/fmars.2020.608032

Arrigo, K. R., Mills, M., Van Dijken, G. L., Lowry, K., Pickart, R., & Schlitzer, R. (2017). Late spring nitrate distributions beneath the ice-covered northeastern Chukchi Shelf. *Journal of Geophysical Research: Biogeosciences*, *122*, 2409–2417. https://doi.org/10.1002/2017JG003881

Arrigo, K. R., Perovich, D. K., Pickart, R. S., Brown, Z. W., Van Dijken, G. L., Lowry, K. E., & Swift, J. H. (2012). Massive phytoplankton blooms under Arctic sea ice. *Science*, *336*, 1408. https://doi.org/10.1126/science.1215065

Arrigo, K. R., Perovich, D. K., Pickart, R. S., Brown, Z. W., Van Dijken, G. L., Lowry, K. E., & Swift, J. H. (2014). Phytoplankton blooms beneath the sea ice in the Chukchi sea. *Deep-Sea Research Part II: Topical Studies in Oceanography*, *105*, 1–16. https://doi.org/10.1016/j.dsr2.2014.03.018

Arrigo, K. R. & Van Dijken, G. L. (2015). Continued increases in Arctic Ocean primary production. *Progress in Oceanography*, *136*, 60–70. https://doi.org/10.1016/j.pocean.2015.05.002

Assmy, P., Fernández-Méndez, M., Duarte, P., Meyer, A., Randelhoff, A., Mundy, C. J., & Granskog, M. A. (2017). Leads in Arctic pack ice enable early phytoplankton blooms below snow-covered sea ice. *Scientific Reports*, *7*(1), 40850. https://doi.org/10.1038/srep40850

Baer, S. E., Sipler, R. E., Roberts, Q. N., Yager, P. L., Frischer, M. E., & Bronk, D. A. (2017). Seasonal nitrogen uptake and regeneration in the western coastal Arctic: Arctic coastal nitrogen dynamics. *Limnology & Oceanography*, *62*(6), 2463–2479. https://doi.org/10.1002/lno.10580

Baumann, M. S., Moran, S. B., Lomas, M. W., Kelly, R. P., & Bell, D. W. (2013). Seasonal decoupling of particulate organic carbon export and net primary production in relation to sea-ice at the shelf break of the eastern Bering Sea: Implications for off-shelf carbon export. *Journal of Geophysical Research*, *118*(10), 5504–5522. https://doi.org/10.1002/jgrc.20366

Blais, M., Tremblay, J.-É., Jungblut, A. D., Gagnon, J., Martin, J., Thaler, M., & Lovejoy, C. (2012). Nitrogen fixation and identification of potential diazotrophs in the Canadian Arctic. *Global Biogeochemical Cycles*, *26*(3), 2011GB004096. https://doi.org/10.1029/2011GB004096

Boetius, A., Albrecht, S., Bakker, K., Bienhold, C., Felden, J., Fernandez-Mendez, M., & Ark27, R. P. (2013). Export of algal biomass from the melting Arctic sea ice. *Science*, *339*(6126), 1430–1432. https://doi.org/10.1126/science.1231346

Boles, E., Provost, C., Garçon, V., Bertosio, C., Athanase, M., Koenig, Z., & Sennéchael, N. (2020). Under-ice phytoplankton blooms in the central Arctic Ocean: Insights from the first biogeochemical IAOOS platform drift in 2017. *Journal of Geophysical Research: Oceans*, *125*(3). https://doi.org/10.1029/2019JC015608

Brown, Z. W., Casciotti, K. L., Pickart, R. S., Swift, J. H., & Arrigo, K. R. (2015). Aspects of the marine nitrogen cycle of the Chukchi Sea shelf and Canada Basin. *Deep-Sea Research Part II: Topical Studies in Oceanography*, *118*, 73–87. https://doi.org/10.1016/j.dsr2.2015.02.009

Burchard, H., Bolding, K., & Ruiz-Villarreal, M. (1999). *GOTM, a general ocean turbulence model. Theory, implementation and test cases*. Space Applications Institute.

Campbell, R. G., Wagner, M., Teegarden, G., Boudreau, C., & Durbin, E. (2001). Growth and development rates of the copepod Calanus finmarchicus reared in the laboratory. *Marine Ecology Progress Series*, *221*, 161–183. https://doi.org/10.3354/meps221161

Carmack, E. & Chapman, D. C. (2003). Wind-driven shelf/basin exchange on an Arctic shelf: The joint roles of ice cover extent and shelf-break bathymetry: Wind-driven shelf/basin exchange. *Geophysical Research Letters*, *30*(14). https://doi.org/10.1029/2003GL017526

Chang, B. X. & Devol, A. H. (2009). Seasonal and spatial patterns of sedimentary denitrification rates in the Chukchi sea. *Deep-Sea Research Part II: Topical Studies in Oceanography*, *56*(17), 1339–1350. https://doi.org/10.1016/j.dsr2.2008.10.024

Conover, R. & Huntley, M. (1991). Copepods in ice-covered seas—distribution, adaptations to seasonally limited food, metabolism, growth patterns and life cycle strategies in polar seas. *Journal of Marine Systems*, *2*(1–2), 1–41. https://doi.org/10.1016/0924-7963(91)90011-I

Coyle, K., Konar, B., Blanchard, A., Highsmith, R., Carroll, J., Carroll, M., & Sirenko, B. (2007). Potential effects of temperature on the benthic infaunal community on the southeastern Bering Sea shelf: Possible impacts of climate change. *Deep Sea Research Part II: Topical Studies in Oceanography*, *54*(23–26), 2885–2905. https://doi.org/10.1016/j.dsr2.2007.08.025

De Robertis, A., Taylor, K., Wilson, C. D., & Farley, E. V. (2017). Abundance and distribution of Arctic cod (Boreogadus saida) and other pelagic fishes over the U.S. Continental shelf of the northern Bering and Chukchi seas. *Deep Sea Research Part II: Topical Studies in Oceanography*, *135*, 51–65. https://doi.org/10.1016/j.dsr2.2016.03.002

Deutsch, C. & Weber, T. (2012). Nutrient ratios as a tracer and driver of ocean biogeochemistry. *Annual Review of Marine Science*, *4*(1), 113–141. https://doi.org/10.1146/annurev-marine-120709-142821

Devol, A. H., Codispotit, L. A., & John, P. (1997). Summer and winter denitrification rates in western Arctic shelf sediments. *Continental Shelf Research*, *17*(9). https://doi.org/10.1016/s0278-4343(97)00003-4

Díez, B., Bergman, B., Pedrós-Alió, C., Antó, M., & Snoeijs, P. (2012). High cyanobacterial nifH gene diversity in Arctic seawater and sea ice brine: Arctic nifH gene diversity. *Environmental Microbiology Reports*, *4*(3), 360–366. https://doi.org/10.1111/j.1758-2229.2012.00343.x

Dobson, F. W. & Smith, S. D. (1988). Bulk models of solar radiation at sea. *Quarterly Journal of the Royal Meteorological Society*, *114*(479), 165–182. https://doi.org/10.1002/qj.49711447909

Ershova, E., Hopcroft, R., Kosobokova, K., Matsuno, K., Nelson, R. J., Yamaguchi, A., & Eisner, L. (2015). Long-term changes in summer zooplankton communities of the western Chukchi Sea, 1945–2012. *Oceanography*, *28*(3), 100–115. https://doi.org/10.5670/oceanog.2015.60

Fahl, K. & Nöthig, E.-M. (2007). Lithogenic and biogenic particle fluxes on the Lomonosov Ridge (central Arctic Ocean) and their relevance for sediment accumulation: Vertical vs. lateral transport. *Deep Sea Research Part I: Oceanographic Research Papers*, *54*(8), 1256–1272. https://doi.org/10.1016/j.dsr.2007.04.014

Fennel, K. (2010). The role of continental shelves in nitrogen and carbon cycling: Northwestern North Atlantic case study. *Ocean Science*, *6*(2), 539–548. https://doi.org/10.5194/os-6-539-2010

Fennel, K., Brady, D., Di Toro, D., Robinson, W., Gardner, W., Giblin, A., & Tobias, C. (2009). Modeling denitrification in aquatic sediments. *Biogeochemistry*, *93*, 159–178. https://doi.org/10.1007/s10533-008-9270-z

Fernández-Méndez, M., Turk-Kubo, K. A., Buttigieg, P. L., Rapp, J. Z., Krumpen, T., Zehr, J. P., & Boetius, A. (2016). Diazotroph diversity in the sea ice, melt ponds, and surface waters of the Eurasian basin of the central Arctic Ocean. *Frontiers in Microbiology*, *7*. https://doi.org/10.3389/fmicb.2016.01884

Fu, W., Randerson, J. T., & Moore, J. K. (2016). Climate change impacts on net primary production (NPP) and export production (EP) regulated by increasing stratification and phytoplankton communitystructure in the CMIP5 models. *Biogeosciences*, *13*(18), 5151–5170. https://doi.org/10.5194/bg-13-5151-2016

Granger, J., Prokopenko, M. G., Sigman, D. M., Mordy, C. W., Morse, Z. M., Morales, L. V., & Plessen, B. (2011). Coupled nitrification-denitrification in sediment of the eastern Bering Sea shelf leads to15N enrichment of fixed N in shelf waters. *Journal of Geophysical Research*, *116*(11), 1–18. https://doi.org/10.1029/2010JC006751

Grebmeier, J. M. (2006). A major ecosystem shift in the northern Bering sea. *Science*, *311*(5766), 1461–1464. https://doi.org/10.1126/science.1121365

Grebmeier, J. M., Bluhm, B., Cooper, L., Denisenko, S., Iken, K., Kedra, M., & Serratos, C. (2015). Time-series benthic community composition and biomass and associated environmental characteristics in the Chukchi Sea during the RUSALCA 2004–2012 program. *Oceanography*, *28*(3), 116–133. https://doi.org/10.5670/oceanog.2015.61

Grebmeier, J. M., McRoy, C., & Feder, H. (1988). Pelagic-benthic coupling on the shelf of the northern Bering and Chukchi Seas. I. Food supply source and benthic bio-mass. *Marine Ecology Progress Series*, *48*, 57–67. https://doi.org/10.3354/meps048057

Gregg, W. W. & Carder, K. L. (1990). A simple spectral solar irradiance model for cloudless maritime atmospheres. *Limnology & Oceanography*, *35*(8), 1657–1675. https://doi.org/10.4319/lo.1990.35.8.1657

Grömping, U. (2006). Relative importance for linear regression in *R*: The package relaimpo. *Journal of Statistical Software*, *17*(1). https://doi.org/10.18637/jss.v017.i01

Gruber, N. & Sarmiento, J. L. (1997). Global patterns of marine nitrogen fixation and denitrification. *Global Biogeochemical Cycles*, *11*(2), 235–266. https://doi.org/10.1029/97GB00077

Hameedi, M. J. (1978). Aspects of water column primary productivity in the Chukchi Sea during summer. *Marine Biology*, *48*(1), 37–46. https://doi.org/10.1007/BF00390529

Hamilton, C., Lydersen, C., Aars, J., Biuw, M., Boltunov, A., Born, E., & Kovacs, K. (2021). Marine mammal hotspots in the Greenland and Barents seas. *Marine Ecology Progress Series*, *659*, 3–28. https://doi.org/10.3354/meps13584

Hansell, D. A., Whitledge, T. E., & Goering, J. J. (1993). Patterns of nitrate utilization and new production over the Bering-Chukchi shelf. *Continental Shelf Research*, *13*(5–6), 601–627. https://doi.org/10.1016/0278-4343(93)90096-G

Henley, S. F., Porter, M., Hobbs, L., Braun, J., Guillaume-Castel, R., Venables, E. J., & Cottier, F. (2020). Nitrate supply and uptake in the Atlantic Arctic sea ice zone: Seasonal cycle, mechanisms and drivers. *Philosophical Transactions of the Royal Society A: Mathematical, Physical & Engineering Sciences*, *378*(2181), 20190361. https://doi.org/10.1098/rsta.2019.0361

Hill, V. J., Ardyna, M., Lee, S. H., & Varela, D. E. (2018). Decadal trends in phytoplankton production in the pacific Arctic region from 1950 to 2012. *Deep Sea Research Part II: Topical Studies in Oceanography*, *152*, 82–94. https://doi.org/10.1016/j.dsr2.2016.12.015

Hill, V. J. & Cota, G. (2005). Spatial patterns of primary production on the shelf, slope and basin of the Western Arctic in 2002. *Deep-Sea Research Part II: Topical Studies in Oceanography*, *52*(24–26), 3344–3354. https://doi.org/10.1016/j.dsr2.2005.10.001

Hill, V. J., Light, B., Steele, M., & Zimmerman, R. C. (2018). Light availability and phytoplankton growth beneath Arctic sea ice: Integrating observations and modeling. *Journal of Geophysical Research: Oceans*, *123*(5), 3651–3667. https://doi.org/10.1029/2017JC013617

Honjo, S., Krishfield, R. A., Eglinton, T. I., Manganini, S. J., Kemp, J. N., Doherty, K., & Takizawa, T. (2010). Biological pump processes in the cryopelagic and hemipelagic Arctic Ocean: Canada basin and Chukchi rise. *Progress in Oceanography*, *85*(3–4), 137–170. https://doi.org/10.1016/j.pocean.2010.02.009

Horak, R. E., Whitney, H., Shull, D. H., Mordy, C. W., & Devol, A. H. (2013). The role of sediments on the Bering Sea shelf N cycle: Insights from measurements of benthic denitrification and benthic DIN fluxes. *Deep-Sea Research Part II: Topical Studies in Oceanography*, *94*, 95–105. https://doi.org/10.1016/j.dsr2.2013.03.014

Horvat, C., Jones, D. R., Iams, S., Schroeder, D., Flocco, D., & Feltham, D. (2017). The frequency and extent of sub-ice phytoplankton blooms in the Arctic Ocean. *Science Advances*, *3*(3). https://doi.org/10.1126/sciadv.1601191

Huntley, M. & Lopez, M. (1992). Temperature-dependent production of marine copepods: A global synthesis. *The American Naturalist*, *140*(2), 201–242. https://doi.org/10.1086/285410

Joiris, C. R. (2011). A major feeding ground for cetaceans and seabirds in the south-western Greenland Sea. *Polar Biology*, *34*(10), 1597–1607. https://doi.org/10.1007/s00300-011-1022-1

Krisch, S., Browning, T. J., Graeve, M., Ludwichowski, K.-U., Lodeiro, P., Hopwood, M. J., & Achterberg, E. P. (2020). The influence of Arctic Fe and Atlantic fixed N on summertime primary production in fram strait, north Greenland sea. *Scientific Reports*, *10*(1), 15230. https://doi.org/10.1038/s41598-020-72100-9

Kuletz, K. J., Ferguson, M. C., Hurley, B., Gall, A. E., Labunski, E. A., & Morgan, T. C. (2015). Seasonal spatial patterns in seabird and marine mammal distribution in the eastern Chukchi and western Beaufort seas: Identifying biologically important pelagic areas. *Progress in Oceanography*, *136*, 175–200. https://doi.org/10.1016/j.pocean.2015.05.012

Kwok, R. (2018). Arctic sea ice thickness, volume, and multiyear ice coverage: Losses and coupled variability (1958-2018). *Environmental Research Letters*, *13*, 105005. https://doi.org/10.1088/1748-9326/aae3ec

Lalande, C., Grebmeier, J. M., Hopcroft, R. R., & Danielson, S. L. (2020). Annual cycle of export fluxes of biogenic matter near Hanna Shoal in the northeast Chukchi Sea. *Deep Sea Research Part II: Topical Studies in Oceanography*, *177*, 104730. https://doi.org/10.1016/j.dsr2.2020.104730

Lalande, C., Grebmeier, J. M., Wassmann, P., Cooper, L. W., Flint, M. V., & Sergeeva, V. M. (2007). Export fluxes of biogenic matter in the presence and absence of seasonal sea ice cover in the Chukchi Sea. *Continental Shelf Research*, *27*(15), 2051–2065. https://doi.org/10.1016/j.csr.2007.05.005

Laney, S. R. & Sosik, H. M. (2014). Phytoplankton assemblage structure in and around a massive under-ice bloom in the Chukchi Sea. *Deep Sea Research Part II: Topical Studies in Oceanography*, *105*, 30–41. https://doi.org/10.1016/j.dsr2.2014.03.012

Laurent, A., Fennel, K., Wilson, R., Lehrter, J., & Devereux, R. (2016). Parameterization of biogeochemical sediment–water fluxes using in situ measurements and a diagenetic model. *Biogeosciences*, *13*(1), 77–94. https://doi.org/10.5194/bg-13-77-2016

Lee, S. H., Whitledge, T. E., & Kang, S.-H. (2007). Recent carbon and nitrogen uptake rates of phytoplankton in Bering Strait and the Chukchi Sea. *Continental Shelf Research*, *27*(17), 2231–2249. https://doi.org/10.1016/j.csr.2007.05.009

Leu, E., Søreide, J., Hessen, D., Falk-Petersen, S., & Berge, J. (2011). Consequences of changing sea-ice cover for primary and secondary producers in the European Arctic shelf seas: Timing, quantity, and quality. *Progress in Oceanography*, *90*(1–4), 18–32. https://doi.org/10.1016/j.pocean.2011.02.004

Lewis, K. M., Van Dijken, G. L., & Arrigo, K. R. (2020). Changes in phytoplankton concentration now drive increased Arctic Ocean primary production. *Science*, *369*(6500), 198–202. https://doi.org/10.1126/science.aay8380

Li, W. K., McLaughlin, F. A., Lovejoy, C., & Carmack, E. C. (2009). Smallest algae thrive as the Arctic Ocean freshens. *Science*, *326*(5952), 539. https://doi.org/10.1126/science.1179798

Liston, G. E., Itkin, P., Stroeve, J., Tschudi, M., Stewart, J. S., Pedersen, S. H., & Elder, K. (2020). A Lagrangian snow-evolution system for sea-ice Applications (SnowModel-LG): Part I—model description. *Journal of Geophysical Research: Oceans*, *125*(10), e2019JC015913. https://doi.org/10.1029/2019JC015913

Logerwell, E., Busby, M., Carothers, C., Cotton, S., Duffy-Anderson, J., Farley, E., & Sformo, T. (2015). Fish communities across a spectrum of habitats in the western Beaufort Sea and Chukchi Sea. *Progress in Oceanography*, *136*, 115–132. https://doi.org/10.1016/j.pocean.2015.05.013

Lowry, K. E., Van Dijken, G. L., & Arrigo, K. R. (2014). Evidence of under-ice phytoplankton blooms in the Chukchi Sea from 1998 to 2012. *Deep-Sea Research Part II: Topical Studies in Oceanography*, *105*, 105–117. https://doi.org/10.1016/j.dsr2.2014.03.013

McLaughlin, F. A. & Carmack, E. C. (2010). Deepening of the nutricline and chlorophyll maximum in the Canada Basin interior, 2003–2009. *Geophysical Research Letters*, *37*(24). https://doi.org/10.1029/2010gl045459

McTigue, N. D., Gardner, W. S., Dunton, K. H., & Hardison, A. K. (2016). Biotic and abiotic controls on co-occurring nitrogen cycling processes in shallow Arctic shelf sediments. *Nature Communications*, *7*(1), 13145. https://doi.org/10.1038/ncomms13145

Meier, W. N., Fetterer, F., Savoie, M., Mallory, S., Duerr, R., & Stroeve, J. (2019). NOAA/NSIDC climate data record of passive microwave sea ice concentration, Version 3. NSIDC: National Snow and Ice Data Center. https://doi.org/10.7265/N59P2ZTG

Mills, M. M., Brown, Z. W., Lowry, K. E., Van Dijken, G. L., Becker, S., Pal, S., & Arrigo, K. R. (2015). Impacts of low phytoplankton NO3-:PO43- utilization ratios over the Chukchi shelf, Arctic Ocean. *Deep Sea Research Part II: Topical Studies in Oceanography*, *118*, 105–121. https://doi.org/10.1016/j.dsr2.2015.02.007

Moisander, P. H., Beinart, R. A., Hewson, I., White, A. E., Johnson, K. S., Carlson, C. A., & Zehr, J. P. (2010). Unicellular cyanobacterial distributions Broaden the oceanic N2 fixation domain. *Science*, *327*(5972), 1512–1514. https://doi.org/10.1126/science.1185468

Moore, S. E. & Kuletz, K. J. (2019). Marine birds and mammals as ecosystem sentinels in and near Distributed biological observatory regions: An abbreviated review of published accounts and recommendations for integration to ocean observatories. *Deep Sea Research Part II: Topical Studies in Oceanography*, *162*, 211–217. https://doi.org/10.1016/j.dsr2.2018.09.004

Mordy, C. W., Bell, S., Cokelet, E. D., Ladd, C., Lebon, G., Proctor, P., & Wood, K. (2020). Seasonal and interannual variability of nitrate in the eastern Chukchi Sea: Transport and winter replenishment. *Deep Sea Research Part II: Topical Studies in Oceanography*, *177*. https://doi.org/10.1016/j.dsr2.2020.104807

Mulholland, M. R., Bernhardt, P. W., Blanco-Garcia, J. L., Mannino, A., Hyde, K., Mondragon, E., & Zehr, J. P. (2012). Rates of dinitrogen fixation and the abundance of diazotrophs in North American coastal waters between Cape Hatteras and Georges Bank. *Limnology & Oceanography*, *57*(4), 1067–1083. https://doi.org/10.4319/lo.2012.57.4.1067

Mundy, C. J., Gosselin, M., Ehn, J., Gratton, Y., Rossnagel, A., Barber, D. G., & Papakyriakou, T. (2009). Contribution of under-ice primary production to an ice-edge upwelling phytoplankton bloom in the Canadian Beaufort Sea. *Geophysical Research Letters*, *36*(17), L17601. https://doi.org/10.1029/2009GL038837

Mundy, C. J., Gosselin, M., Gratton, Y., Brown, K., Galindo, V., Campbell, K., & Bélanger, S. (2014). Role of environmental factors on phytoplankton bloom initiation under landfast sea ice in Resolute Passage, Canada. *Marine Ecology Progress Series*, *497*, 39–49. https://doi.org/10.3354/meps10587

Munk, P. (2003). Changes in plankton and fish larvae communities across hydrographic fronts off West Greenland. *Journal of Plankton Research*, *25*(7), 815–830. https://doi.org/10.1093/plankt/25.7.815

Nummelin, A., Ilicak, M., Li, C., & Smedsrud, L. H. (2016). Consequences of future increased Arctic runoff on Arctic Ocean stratification, circulation, and sea ice cover. *Journal of Geophysical Research: Oceans*, *121*(1), 617–637. https://doi.org/10.1002/2015JC011156

Oziel, L., Massicotte, P., Randelhoff, A., Ferland, J., Vladoiu, A., Lacour, L., & Babin, M. (2019). Environmental factors influencing the seasonal dynamics of spring algal blooms in and beneath sea ice in western Baffin Bay. *Elementa: Science of the Anthropocene*, *7*, 34. https://doi.org/10.1525/elementa.372

Payne, C. M., Bianucci, L., Dijken, G. L., & Arrigo, K. R. (2021). Changes in under-ice primary production in the Chukchi Sea from 1988 to 2018. *Journal of Geophysical Research: Oceans*, *126*(9). https://doi.org/10.1029/2021JC017483

Peng, G., Meier, W. N., Scott, D. J., & Savoie, M. H. (2013). A long-term and reproducible passive microwave sea ice concentration data record for climate studies and monitoring. *Earth System Science Data*, *8*. https://doi.org/10.5194/essd-5-311-2013

Peralta-Ferriz, C. & Woodgate, R. A. (2017). The dominant role of the East Siberian Sea in driving the oceanic flow through the Bering Strait—conclusions from GRACE ocean mass satellite data and in situ mooring observations between 2002 and 2016. *Geophysical Research Letters*, *44*(22). https://doi.org/10.1002/2017GL075179

Perrette, M., Yool, A., Quartly, G. D., & Popova, E. E. (2011). Near-ubiquity of ice-edge blooms in the Arctic. *Biogeosciences*, *8*(2), 515–524. https://doi.org/10.5194/bg-8-515-2011

Rainville, L. & Woodgate, R. A. (2009). Observations of internal wave generation in the seasonally ice-free Arctic. *Geophysical Research Letters*, *36*(23), L23604. https://doi.org/10.1029/2009GL041291

Randelhoff, A., Holding, J., Janout, M., Sejr, M. K., Babin, M., Tremblay, J.-É., & Alkire, M. B. (2020). Pan-Arctic Ocean primary production constrained by turbulent nitrate fluxes. *Frontiers in Marine Science*, *7*, 150. https://doi.org/10.3389/fmars.2020.00150

Randelhoff, A., Oziel, L., Massicotte, P., Bécu, G., Galí, M., Lacour, L., & Babin, M. (2019). The evolution of light and vertical mixing across a phytoplankton ice-edge bloom. *Elementa: Science of the Anthropocene*, *7*, 20. https://doi.org/10.1525/elementa.357

Randelhoff, A., Reigstad, M., Chierici, M., Sundfjord, A., Ivanov, V., Cape, M., & Kristiansen, S. (2018). Seasonality of the physical and biogeochemical hydrography in the inflow to the Arctic Ocean through fram strait. *Frontiers in Marine Science*, *5*, 224. https://doi.org/10.3389/fmars.2018.00224

Reynolds, R., Smith, T., Chelton, D. B., Casey, K. S., & Schlax, M. (2007). Daily high-resolution-Blended analyses for sea surface temperature. *Journal of Climate*, *20*(22), 5473–5496. https://doi.org/10.1175/2007jcli1824.1

Rysgaard, S., Nielsen, T., & Hansen, B. (1999). Seasonal variation in nutrients, pelagic primary production and grazing in a high-Arctic coastal marine ecosystem, Young Sound, Northeast Greenland. *Marine Ecology Progress Series*, *179*, 13–25. https://doi.org/10.3354/meps179013

Serreze, M. C. & Stroeve, J. (2015). *Arctic sea ice trends, variability and implications for seasonal ice forecasting* (pp. 20140159). Philosophical Transactions of the Royal Society of London.

Sherr, B. F., Hill, V. J., Plourde, S., Stockwell, D. A., Ashjian, C. J., Sherr, E. B., & Campbell, R. G. (2008). Mesozooplankton prey preference and grazing impact in the western Arctic Ocean. *Deep Sea Research Part II: Topical Studies in Oceanography*, *56*(17), 1274–1289. https://doi.org/10.1016/j.dsr2.2008.10.027

Sherr, E. B., Sherr, B. F., & Hartz, A. J. (2009). Microzooplankton grazing impact in the western Arctic Ocean. *Deep Sea Research Part II: Topical Studies in Oceanography*, *56*(17), 1264–1273. https://doi.org/10.1016/j.dsr2.2008.10.036

Sipler, R. E., Gong, D., Baer, S. E., Sanderson, M. P., Roberts, Q. N., Mulholland, M. R., & Bronk, D. A. (2017). Preliminary estimates of the contribution of Arctic nitrogen fixation to the global nitrogen budget. *Limnology and Oceanography Letters*, *2*(5), 159–166. https://doi.org/10.1002/lol2.10046

Smetacek, V. (1999). Diatoms and the ocean carbon cycle. *Protist*, *150*(1), 25–32. https://doi.org/10.1016/S1434-4610(99)70006-4

Soetaert, K., Herman, P. M., & Middelburg, J. J. (1996a). Dynamic response of deep-sea sediments to seasonal variations: A model. *Limnology & Oceanography*, *41*(8), 1651–1668. https://doi.org/10.4319/lo.1996.41.8.1651

Soetaert, K., Herman, P. M., & Middelburg, J. J. (1996b). A model of early diagenetic proceses from the shelf to abyssal depths. *Geochimica et Cosmochimica Acta*, *60*(6), 1019–1040. https://doi.org/10.1016/0016-7037(96)00013-0

Sohm, J. A., Webb, E. A., & Capone, D. G. (2011). Emerging patterns of marine nitrogen fixation. *Nature Reviews Microbiology*, *9*(7), 499–508. https://doi.org/10.1038/nrmicro2594

Stroeve, J., Liston, G. E., Buzzard, S., Zhou, L., Mallett, R., Barrett, A., & Stewart, J. S. (2020). A Lagrangian snow evolution system for sea ice applications (SnowModel-LG): Part II—Analyses. *Journal of Geophysical Research: Oceans*, *125*(10). https://doi.org/10.1029/2019JC015900

Stroeve, J., Markus, T., Boisvert, L., Miller, J., & Barrett, A. (2014). Changes in Arctic melt season and its implications for sea ice loss. *Geophysical Research Letters*, *41*, 1216–1225. https://doi.org/10.1002/2013GL058951.Received

Szymanski, A. & Gradinger, R. (2016). The diversity, abundance and fate of ice algae and phytoplankton in the Bering Sea. *Polar Biology*, *39*(2), 309–325. https://doi.org/10.1007/s00300-015-1783-z

Townsend, D. W. & Cammen, L. M. (1988). Potential importance of the timing of spring plankton blooms to benthic-pelagic coupling and recruitment of juvenile demersal fishes. *Biological Oceanography*, *5*(13), 215–228.

Tremblay, J.-É., Bélanger, S., Barber, D. G., Asplin, M., Martin, J., Darnis, G., & Gosselin, M. (2011). Climate forcing multiplies biological productivity in the coastal Arctic Ocean. *Geophysical Research Letters*, *38*(18). https://doi.org/10.1029/2011gl048825

Tremblay, J.-É. & Gagnon, J. (2009). The effects of irradiance and nutrient supply on the productivity of Arctic waters: A perspective on climate change. In J. C. J. Nihoul, & A. G. Kostianoy (Eds.), *Influence of climate change on the changing Arctic and sub-Arctic conditions* (pp. 73–93). Springer. https://doi.org/10.1007/978-1-4020-9460-6_7

Tschudi, M., Meier, W. N., Stewart, J. S., Fowler, C., & Maslanik, J. (2019). EASE-grid sea ice age, version 4. NASA national snow and ice data center DAAC.

Tsujii, K., Otsuki, M., Akamatsu, T., Matsuo, I., Amakasu, K., Kitamura, M., & Mitani, Y. (2016). The migration of fin whales into the southern Chukchi Sea as monitored with passive acoustics. *ICES Journal of Marine Science*, *73*(8), 2085–2092. https://doi.org/10.1093/icesjms/fsv271

Webster, M. A., Rigor, I. G., Perovich, D. K., Richter-Menge, J. A., Polashenski, C. M., & Light, B. (2015). Seasonal evolution of melt ponds on Arctic sea ice. *Journal of Geophysical Research: Oceans*, *120*(9), 5968–5982. https://doi.org/10.1002/2015JC011030

Woodgate, R. A. (2018). Increases in the Pacific inflow to the Arctic from 1990 to 2015, and insights into seasonal trends and driving mechanisms from year-round Bering Strait mooring data. *Progress in Oceanography*, *160*, 124–154. https://doi.org/10.1016/j.pocean.2017.12.007

Woodgate, R. A., Aagaard, K., & Weingartner, T. J. (2005). A year in the physical oceanography of the Chukchi Sea: Moored measurements from autumn 1990–1991. *Deep Sea Research Part II: Topical Studies in Oceanography*, *52*(24–26), 3116–3149. https://doi.org/10.1016/j.dsr2.2005.10.016

Yamamoto-Kawai, M., Carmack, E., & McLaughlin, F. (2006). Nitrogen balance and Arctic throughflow. *Nature*, *443*(7107), 43. https://doi.org/10.1038/443043a

Yang, J. (2004). Storm-driven mixing and potential impact on the Arctic Ocean. *Journal of Geophysical Research*, *109*(C4), C04008. https://doi.org/10.1029/2001JC001248

Zhang, J., Spitz, Y. H., Steele, M., Ashjian, C., Campbell, R., Berline, L., & Matrai, P. (2010). Modeling the impact of declining sea ice on the Arctic marine planktonic ecosystem. *Journal of Geophysical Research*, *115*(C10), C10015. https://doi.org/10.1029/2009JC005387

Zhou, L., Stroeve, J., Xu, S., Petty, A., Tilling, R., Winstrup, M., & Nandan, V. (2021). Inter-comparison of snow depth over Arctic sea ice from reanalysis reconstructions and satellite retrieval. *The Cryosphere*, *15*(1), 345–367. https://doi.org/10.5194/tc-15-345-2021